GAIN DEGRADATION AND AMPLITUDE SCINTILLATION DUE TO TROPOSPHERIC TURBULENCE

D.M. Theobold and D.B. Hodge

The Ohio State University
ElectroScience Laboratory
Department of Electrical Engineering
Columbus, Ohio 43212

Technical Report 784299-6

February 1978

Revised Edition
June 1978

Prepared for
National Aeronautics and Space Administration
GODDARD SPACE FLIGHT CENTER
Greenbelt, Maryland 20771

NOTICES

When Government drawings, specifications, or other data are used for any purpose other than in connection with a definitely related Government procurement operation, the United States Government thereby incurs no responsibility nor any obligation whatsoever, and the fact that the Government may have formulated, furnished, or in any way supplied the said drawings, specifications, or other data, is not to be regarded by implication or otherwise as in any manner licensing the holder or any other person or corporation, or conveying any rights or permission to manufacture, use, or sell any patented invention that may in any way be related thereto.

TECHNICAL REPORT STANDARD TITLE PAGE

1. Report No.	2. Government Accession No.	3. Recipient's Catalog No.

4. Title and Subtitle	5. Report Date
GAIN DEGRADATION AND AMPLITUDE SCINTILLATION DUE TO TROPOSPHERIC TURBULENCE	February 1978 (June 78)
	6. Performing Organization Code
7. Author(s)	8. Performing Organization Report No.
D. M. Theobold and D. B. Hodge	ESL 784299-6 (revised)
9. Performing Organization Name and Address	10. Work Unit No.
The Ohio State University ElectroScience Laboratory, Department of Electrical Engineering, Columbus, Ohio 43212	
	11. Contract or Grant No.
	NAS5-22575
	13. Type of Report and Period Covered
12. Sponsoring Agency Name and Address	Type II Technical Report
NASA, GSFC Greenbelt, Maryland 20771 E. Hirschmann, Code 951, Technical Officer	14. Sponsoring Agency Code

15. Supplementary Notes

This material was also used as a dissertation submitted to The Ohio State University.

16. Abstract

Mean signal levels well below those predicted by standard techniques on low elevation earth-space microwave links have been observed and reported previously. Additionally, amplitude fluctuations under clear air conditions accompany these reduced signal levels and increase significantly as elevation angle decreases. It is shown that a simple physical model is adequate for the prediction of the long term statistics of both the reduced signal levels and increased peak-to-peak fluctuations. The model is based on conventional atmospheric turbulence theory and incorporates both amplitude and angle of arrival fluctuations.

Angle of arrival statistics were compiled from previous and current experiments; and these results were used to establish an empirical relationship between the long term average angle of arrival variance and either path length for terrestrial paths or elevation angle for earth-space paths. Secondly, the relationship between turbulence induced amplitude fluctuations and path length previously derived in the work of V. I. Tatarski and verified by measured data

17. Key Words (Selected by Author(s))	18. Distribution Statement
Microwave Gain degradation Amplitude scintillation Angle of arrival	

19. Security Classif. (of this report)	20. Security Classif. (of this page)	21. No. of Pages	22. Price*
U	U	55	

*For sale by the Clearinghouse for Federal Scientific and Technical Information, Springfield, Virginia 22151.

16.

has also been utilized.

It is hypothesized that a plane wave propagating through the troposphere is perturbed by the two coupled statistical processes mentioned above. This perturbed plane wave is then received by a finite aperture antenna having a Gaussian power pattern. The average realized gain is then calculated accounting for the angle of arrival fluctuations. The resulting average gain degradation, when combined with the usual atmospheric gas absorption, adequately predicts the reduced long term signal levels observed at low elevation angles on earth-space paths at 2, 7.3 and 30 GHz. The expected value of the variance of the received signal amplitude fluctuations is calculated by combining the amplitude and angle of arrival statistics of the incident wave with the receiver characteristics. This model predicts the average variance of signals observed under clear air conditions at low elevation angles on earth-space paths at 2, 7.3, 20 and 30 GHz.

Design curves based on this model for gain degradation, realizable gain, and amplitude fluctuation as a function of antenna aperture size, frequency, and either terrestrial path length or earth-space path elevation angle are presented.

17.

Turbulence
Propagation
Earth-Space
Low elevation angle

FOREWORD

The propagation of electromagnetic and acoustic waves in media whose constitutive parameters are random functions of time and space has become a topic of increasing interest. Terrestrial line of sight and earth-space microwave propagation paths traverse the troposphere, where fluctuations in temperature, pressure, and water content produce random variations in the electromagnetic properties. The resulting effects are generally more pronounced with increasing frequency and larger path lengths. Communications technology continually progresses higher in frequency and bandwidth in search of greater information rates, long atmospheric path lengths are necessarily employed as satellites come into common usage for communications relays, and remote sensing of meteorological, terrestrial, or airborne phenomena requires electromagnetic propagation through long distances in the atmosphere. The design of each of these potential or current technologies requires knowledge of the interaction between the turbulent atmosphere and wave propagation based upon a realistic model of the turbulence and its consequences.

The work of V. I. Tatarski [1] in 1961 appears to be the first to form a broad theoretical basis for plane wave propagation through a turbulent atmosphere. His amplitude fluctuation and power spectrum results were extended in 1971 to include phase and differential phase variation [2]. The work of Schmeltzer [3] extended this work to form a basis for spherical-wave, finite-aperture cases. Both sets of work employed the Rytov method and its inherent restrictions that the magnitude of fluctuations on the wave be small and that all refractive perturbations be large compared to wavelength. In 1969, Lee and Harp [4] applied a phase screen technique to this problem which permitted generalized amplitude and phase fluctuation expressions to include finite antenna apertures, focused beam waves, medium losses, and atmospheric anisotropy. This technique, which has a primarily physical rather than mathematical basis, allows the Rytov restriction of large perturbations relative to wavelength to be relaxed. Either or both methods have been variously employed by Clifford [5], Ishimaru [6], and Mandics, Lee, and Waterman [7] to obtain temporal frequency spectra. The extension of turbulence theory to account for strong fluctuations and explain the optical saturation phenomena was made by Gracheva and Gurvich [8] in 1965.

Excellent summaries of the above work and reviews of current work are available [1,2,9-13]. The recent summary by A. Ishimaru [13] contains a particularly good bibliography of theoretical and experimental papers.

In principal, theoretical work in this field may be verified by experiment, and a great deal of effort has been made to do so. Experiments must be structured carefully such that all relative physical parameters are measured and no false assumptions are made about the measurement equipment or the medium. Because of the statistical nature of the measurement problem, limited temporal measurements of quantities such as amplitude, absolute, or differential phase do not adequately characterize random media propagation effects from the systems application viewpoint. Communications link design requires long term time characterization in the form of amplitude, phase, spectral, and coherency distributions. The work which follows presents a long term, time average, statistical model with empirical constants for microwave propagation through the turbulent troposphere. Amplitude and differential phase statistics are specifically addressed, but the techniques may be extended to spectral and coherency characterizations.

The material contained in this report is also used as a dissertation submitted to the Department of Electrical Engineering, The Ohio State University as partial fulfillment for the degree Doctor of Philosophy.

TABLE OF CONTENTS

LIST OF TABLES

LIST OF FIGURES

INTRODUCTION

The propagation of electromagnetic and acoustic waves in media whose constitutive parameters are random functions of time and space has become a topic of increasing interest. Terrestrial line of sight and earth-space microwave propagation paths traverse the troposphere, where fluctuations in temperature, pressure, and water content produce random variations in the electromagnetic properties. The resulting effects are generally more pronounced with increasing frequency and larger path lengths. Communications technology continually progresses higher in frequency and bandwidth in search of greater information rates, long atmospheric path lengths are necessarily employed as satellites came into common useage for communications relays, and remote sensing of meteorological, terrestrial, or airborne phenomena requires electromagnetic propagation through long distances in the atmosphere. The design of each of these potential or current technologies requires knowledge of the interaction between the turbulent atmosphere and wave propagation based upon a realistic model of the turbulence and its consequences.

The work of V. I. Tatarski [1] in 1961 appears to be the first to form a broad theoretical basis for plane wave propagation through a turbulent atmosphere. His amplitude fluctuation and power spectrum results were extended in 1971 to include phase and differential phase variation [2]. The work of Schmeltzer [3] extended this work to form a basis for spherical-wave, finite-aperture cases. Both sets of work employed the Rytov method and its inherent restrictions that the magnitude of fluctuations on the wave be small and that all refractive perturbations be large compared to wavelength. In 1969, Lee and Harp [4] applied a phase screen technique to this problem which permitted generalized amplitude and phase fluctuation expressions to include finite antenna apertures, focused beam waves, medium losses, and atmospheric anisotropy. This technique, which has a primarily

physical rather than mathematical basis, allows the Rytov restriction of large perturbations relative to wavelength to be relaxed. Either or both methods have been variously employed by Clifford [5], Ishimaru [6], and Mandics, Lee, and Waterman [7] to obtain temporal frequency spectra. The extension of turbulence theory to account for strong fluctuations and explain the optical saturation phenomena was made by Gracheva and Gurvich [8] in 1965.

Excellent summaries of the above work and reviews of current work are available [1,2,9-13]. The recent summary by A. Ishimaru [13] contains a particularly good bibliography of theoretical and experimental papers.

In principal, theoretical work in this field may be verified by experiment, and a great deal of effort has been made to do so. Experiments must be structured carefully such that all relative physical parameters are measured and no false assumptions are made about the measurement equipment or the medium. Because of the statistical nature of the measurement problem, limited temporal measurements of quantities such as amplitude, absolute, or differential phase do not adequately characterize random media propagation effects from the systems application viewpoint. Communications link design requires long term time characterization in the form of amplitude, phase, spectral, and coherency distributions. The paper which follows presents a long term, time average, statistical model with empirical constants for microwave propagation through the turbulent troposphere. Amplitude and differential phase statistics are specifically addressed, but the techniques may be extended to spectral and coherency characterizations.

CHAPTER I
METHOD

As millimeter wave systems are applied to earth-space and terrestrial communications links, the designer must be aware that certain propagation phenomena which were negligible at lower frequencies will have pronounced effects on link characteristics. For example, a larger aperture which adds gain to the link equation at high elevation angle on an earth-space path may provide less gain than expected if employed at low angles. Similarly, clear air amplitude scintillations which may be neglected at decimeter wavelengths on a long unobstructed terrestrial path may be quite significant at millimeter wavelengths.

The temporal behavior of the signal is less important than its statistical properties when one is interested in link reliability. The long term time average behavior of signal level and variance are the most useful design criteria for a communication link which must be continuously operational over a period of years. A propagation model must predict this long term average behavior and provide a statistical measure of expected deviation from that mean in terms of long term probability distribution functions.

Refractive irregularities in the troposphere due to turbulence, humidity, and temperature gradients affect the propagation of electromagnetic waves of centimeter and shorter wavelengths quite markedly on long terrestrial propagation paths or on earth-space paths with small elevation angles. As a plane wave traverses the atmosphere, changes in refractive index due to turbulence, i.e., ripple or tilt, will perturb the phase front, induce amplitude changes by focusing effects, and scatter energy away from the propagation path. The following discussion will deal only with clear air effects and thus energy scattered out of the beamwidth of an antenna will be considered negligible compared to the energy received. Frequencies of interest

will range from roughly 1 to 100 GHz, which are sufficiently high that ionospheric effects may be neglected except in rare instances.

The statistics of the perturbed wave are modelled by theoretical expressions matched to experimental observations. The perturbed wave impinges on a finite aperture antenna, whose response is a received signal with amplitude diminished from that expected for a free-space path and fluctuating in amplitude.

An expression for the incident wave, the manner in which it attenuates and decomposes into amplitude and angle varying components and the transfer function of the receiving antenna will now be presented.

CHAPTER II
STATISTICAL MODEL

An unperturbed plane wave will be considered incident on a turbulent medium at position z=0 (Figure 1). Propagation within the turbulence and the resulting perturbations of the signal continue until the wave impinges on a receiving aperture at Z=L. The incident plane wave decomposes into two uncoupled components as it traverses the region of turbulence.

The first component, with magnitude f_1, varies in amplitude and is constant in angle. All of the plane wave energy is contained in f_1 at z=0, and its amplitude fluctuation is very small at the beginning of the turbulent region. As this component penetrates deeper into the turbulence, it loses energy to the second component and its peak-to-peak amplitude fluctuations become a larger percentage of its own remaining energy.

The second component, having magnitude f_2, is constant in amplitude at any given position z and it varies in angle or direction of propagation. f_2 contains no energy at z=0 and at the beginning of the region of turbulence it is small in amplitude and has small fluctuations in angle. As this component penetrates into the turbulence it acquires energy at the expense of the amplitude varying component, f_1, and its peak-to-peak angle fluctuations increase.

This concept of constant angle and constant amplitude components which are uncoupled corresponds to Ishimaru's discussion of coherent and incoherent waves (Reference [13], pp. 1046-1047) for line of sight propagation through randomly distributed particles. The constant angle, varying amplitude intensity $\langle f_1^2 \rangle$ corresponds to

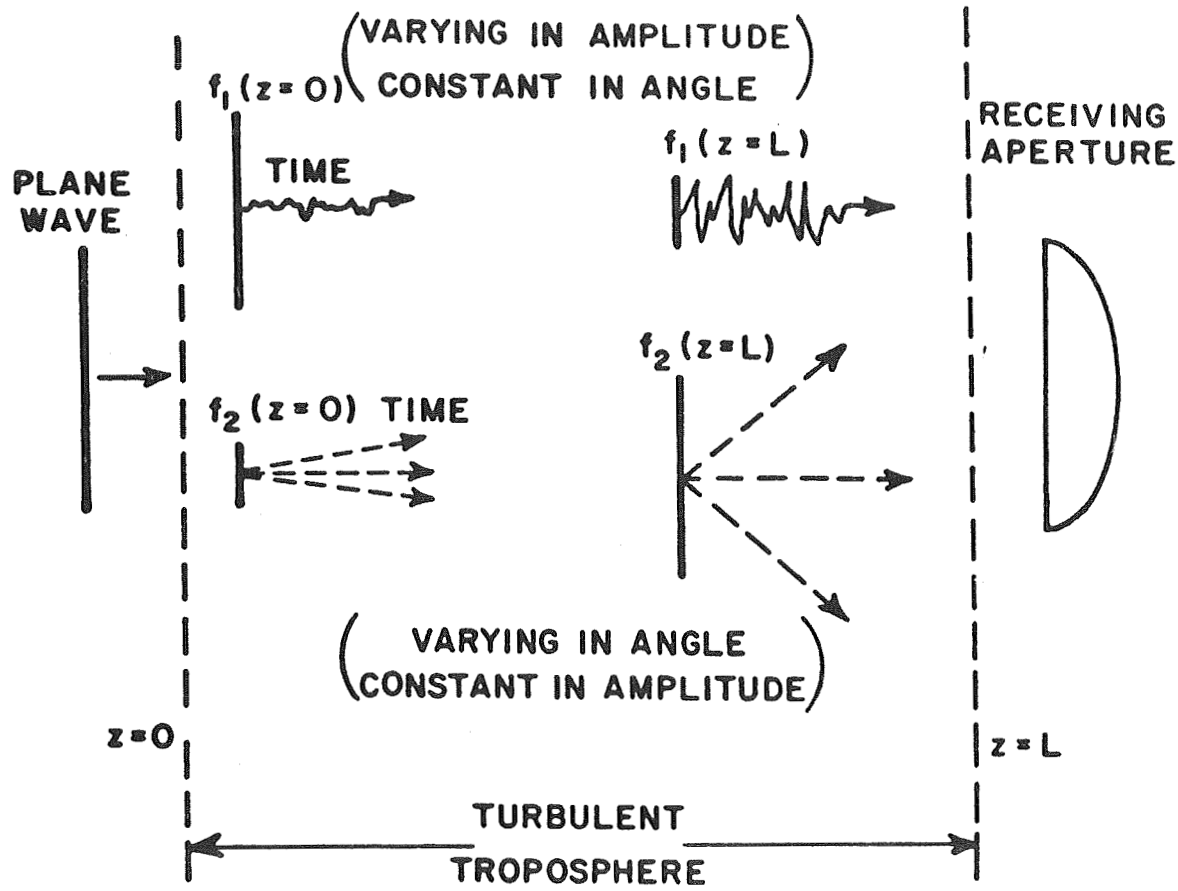

Figure 1. Plane wave decomposition.

Ishimaru's coherent intensity, I_c. Also, the constant amplitude, varying angle intensity $\langle f_2^2 \rangle$ corresponds to his incoherent intensity, I_i.

The magnitude of the electric field component, E_i, of a perturbed plane wave incident on a receiving aperture is a random function of time, varying in amplitude and phase

$$\tilde{E}_i = C[\tilde{f}_1 \cos(\omega_o t + \xi_o + \tilde{\xi}_1 - \vec{\beta}_o \cdot \vec{r}) + f_2 \cos(\omega_o t + \xi_o + \tilde{\xi}_2 - \vec{\beta}_\alpha \cdot \vec{r})] \qquad (1)$$

Random variables are denoted by tilde, and C represents the average magnitude of an incident plane wave, including free space path loss and gas absorption, after propagating through some length, L, of turbulent medium. f_1 and f_2 are magnitude components representing the decomposition, as a function of distance, of the original wave into amplitude and angle of arrival varying parts, respectively. The frequency of the wave is ω_o, ξ_o is the mean absolute phase between the transmitter and receiver, and $\tilde{\xi}_1$ and $\tilde{\xi}_2$ are random variables representing fluctuations in apparent path length. It is assumed that scattering out of the path does not occur and that the random amplitude and angle of arrival processes are conservative in intensity, i.e.,

$$\langle \tilde{f}_1^2 \rangle + f_2^2 = 1 \qquad (2)$$

where $\langle\ \rangle$ denotes the ensemble average over amplitude and angle. Note that total intensity is one, that is, it is normalized to power density at any position along the path. This normalization is justified because the factor C in Equation (1) contains free space and gas absorption terms which equally affect f_1 and f_2. In addition, it will later be shown that the amplitude process $\langle \tilde{f}_1^2 \rangle$ further splits into an average and fluctuating part for the case of strong turbulence. The mean power in the amplitude component

will take on the form $\langle \tilde{f}_1^2 \rangle = \bar{f}_1^2(1+\sigma_1^2)$, where σ_1^2 is amplitude variance and $\bar{f}_1$ is the statistical mean of $\tilde{f}_1$. This is simply a statement that, for $\tilde{f}_1$, the peak to peak fluctuation increases at the expense of power in the mean, as we saw in the sketch of $f_1(Z=L)$ in Figure 1. $\vec{\beta}$ is the vector propagation constant, where the subscripts 0 and α denote the direction of propagation relative to the beam axis. $\vec{r}$ is the position vector.

The receiver will be assumed linear, with ideal bandpass characteristics, and does not maintain absolute phase coherence. If a square-law device is employed as the first mixer, the receiver output voltage will be (see Appendix I)

$$\tilde{v} = \frac{\lambda}{\sqrt{4\pi}} \, C\left|\tilde{f}_1 G(0)\exp(-i\tilde{\xi}_1)+f_2 G(\tilde{\alpha})\exp(-i\tilde{\xi}_2)\right| . \qquad (3)$$

Note that absolute phase is lost and the $\omega_0 t$ time dependence is effectively integrated by the bandwidth of the receiver. $G(\alpha)$ is the directive gain of the antenna as a function of the angle of arrival, α, measured with respect to the beam axis.

The first and second moments of $\tilde{v}$, namely mean $\langle \tilde{v} \rangle$ and second moment $\langle \tilde{v}^2 \rangle$, must be obtained in order to characterize received signal variance and gain degradation. Hence, the statistical properties of $\tilde{f}_1$, $\tilde{\alpha}$, $\tilde{\xi}_1$, and $\tilde{\xi}_2$ must be used since they comprise the expression for $\tilde{v}$. f_1 and f_2 are amplitudes of the two components and $\tilde{\xi}_1$ and $\tilde{\xi}_2$ are their respective relative phases. In the following, η and α will denote the random variable spaces in amplitude and angle of arrival, respectively.

Define $\tilde{\alpha}$ as an angle of arrival random variable, referenced to the axis of the receiving antenna beam. Its distribution in angle equals the mass in the circle $\alpha \leq \sqrt{\theta^2+\phi^2}$ of radius α, where θ and ϕ form an orthogonal coordinate system with the axis (see Figure 2). The beam axis is pointed in the mean direction of arrival of the incident

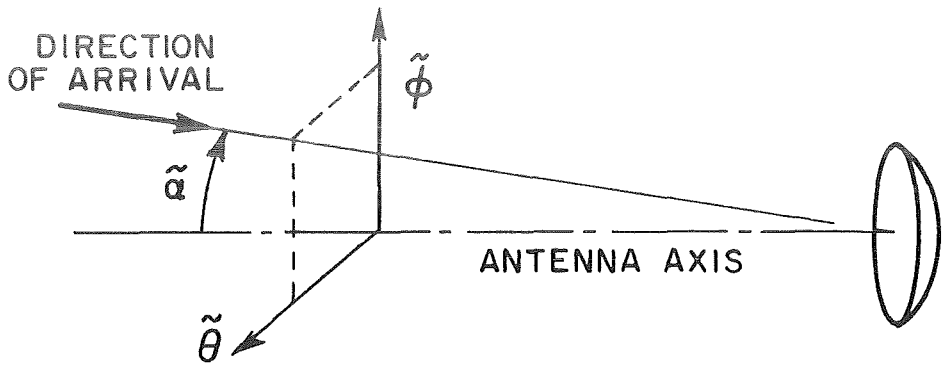

Figure 2. Geometric definitions.

wavefront. Hence $\tilde{\theta}$ and $\tilde{\phi}$ have zero mean angle of arrival. If they are also normal, independent random variables with equal variances ($\sigma_\theta^2=\sigma_\phi^2=\sigma_2^2$), and constant in amplitude dummy variable η, it may be shown [16] that the probability density function, pdf, of the angle varying component of $\tilde{v}$ is then

$$h_2(\alpha,\eta) = h_\alpha(\alpha)\delta(\eta) = \frac{\alpha}{\sigma_2^2}\exp[-\alpha^2/2\sigma_2^2]\delta(\eta); \qquad \alpha \geq 0. \tag{4}$$

The angle varying component f_2 is constant in amplitude, namely $\overline{f}_2$ in amplitude, and hence has zero amplitude variance. The definition of its pdf on the amplitude random variable space with the Dirac delta function $\delta(\eta)$ denotes this fact. The angular fluctuation in α is completely specified by the Rayleigh density function $h_\alpha(\alpha)$, with angular variance parameter σ_2. Independence between the α and η random variable spaces is observed, since $h_2(\alpha,\eta)$ is expressed as a simple product of pdf's, one a function of only α and the other a function of only η.

The random amplitude component $\tilde{f}_1$ has been found to be normally distributed [14]; let its mean be $\overline{f}_1$, its variance σ_1^2, and express its randomness in terms of the amplitude dummy variable, η and the angle of arrival variable, α. The pdf, $h_1(\alpha,\eta)$, of the amplitude varying component, $\tilde{f}_1$, is then assumed to be

$$h_1(\alpha,\eta) = h_\eta(\eta)\delta(\alpha) = \frac{1}{\sqrt{2\pi}\sigma_1}\exp[-(\eta-\overline{f}_1)^2/2\sigma_1^2]\delta(\alpha), \tag{5}$$

where $\delta(\alpha)$ denotes that amplitude varying component $\tilde{f}_1$ is constant in angle of arrival and hence independent of the angle varying component of $\tilde{v}$ [15]. The amplitude fluctuation is expressed by the Gaussian density function $h_\eta(\eta)$ with amplitude mean $\bar{f}_1$ and variance σ_1^2. The assumption of a normal distribution function for $\tilde{f}_1$ is based upon the weak scattering assumption used by Tatarskii and the fact that the statistical behavior of log normal and normal variables is identical for small fluctuations.

Henceforth, the subscript 1 will denote statistical quantities in the amplitude domain η. Likewise, subscript 2 will be used to specify statistical parameters referred to the angle of arrival domain, α. This use of subscripts does not imply, however, that $\tilde{f}_1$ is only defined on amplitude space η, i.e., it carries constant α dependence.

The phase variables $\tilde{\xi}_1$ and $\tilde{\xi}_2$ represent random delay variables caused by apparent fluctuations in path length. For reasonably long path lengths and assuming that all scattering mechanisms are incoherent, the $\tilde{\xi}_1$ and $\tilde{\xi}_2$ random delay variables will fluctuate over many radians and may be considered to be uniformly distributed over $-\pi/2$ to $\pi/2$.

The path length dependence of f_1 and f_2 will now be examined. It has been shown [17] that the variance of the normal direction vector of a plane wave increases linearly with path length when the path length is greater than the correlation radius of the refractivity fluctuations. This condition is certainly met for paths several kilometers long. Additionally, since the axis of the antenna is aligned with the mean angle of arrival, the second moment of the zero-mean angle of arrival component follows the variance behavior of the wavefront direction vector, i.e., $\sigma_2^2 = \langle \tilde{\alpha}^2 \rangle$. A suitable model for the decomposition of an unperturbed wave into incoherent angle of arrival fluctuating components has been suggested in Reference 13, Equation (2-126), to be exponential, with some characteristic decay rate,

say L_o, which is dependent upon the scattering cross section of the turbulence. The expression

$$\tilde{f}_2^2 = 1 - \exp[-L/L_o] \tag{6}$$

combined with (2) will be used as a suitable model for this desired behavior. Also, recall that f_2 varies in angle and is constant in amplitude. Hence, (6) may be rewritten

$$\overline{f_2^2} = 1 - \exp[-L/L_o] = f_2^2 \tag{7}$$

All statistical quantities in the expression for $\tilde{v}$ have now been defined and these definitions will be used to determine the first and second moments of the receiver output voltage,

$$\tilde{v} = \frac{\lambda}{\sqrt{4\pi}} C\left|\sqrt{G(0)}\tilde{f}_1 \exp(-i\tilde{\xi}_1) + \sqrt{G(\tilde{\alpha})}\, f_2 \exp(-i\tilde{\xi}_2)\right|, \tag{8}$$

If B is the beamwidth of the antenna in degrees and $g(\alpha)$ is the pattern factor, then

$$G(\alpha) = g(\alpha)\,(180)^2/B^2 \quad \text{and} \tag{9}$$

$$\tilde{v} = \frac{180\lambda}{B\sqrt{4\pi}} C\Big|g(0)\tilde{f}_1^2 + g(\tilde{\alpha})f_2^2 + \sqrt{g(0)g(\tilde{\alpha})}\tilde{f}_1 f_2 \exp(-i\tilde{\xi}_1 + i\tilde{\xi}_2) + \sqrt{g(0)g(\tilde{\alpha})}\tilde{f}_1 f_2 \exp(+i\tilde{\xi}_1 - i\tilde{\xi}_2)\Big|^{1/2} . \tag{10}$$

Assume a representative pattern factor for a narrow beam, circularly symmetric beam with 3 dB beamwidth, B, to be

$$g(\alpha) = \exp\left[\frac{-\alpha^2 4 \ln 2}{B^2}\right] . \tag{11}$$

The first moment of $\tilde{v}$ is found by integrating (10) and the pdf $h_1(\alpha,\eta)$ and pdf $h_2(\alpha,\eta)$ times variables containing $\tilde{f}_1$ and f_2, respectively. Integration on amplitude variable η is taken over $-\infty$ to ∞ and on angle variable α from 0 to π. The phase variables ξ_1 and ξ_2 are uniformly distributed over $-\pi/2$ to $\pi/2$ and hence

the integration of the last terms in (10) is nearly zero (see Appendix B). This integration reduces the first moment to the form

$$\langle \tilde{v} \rangle = \frac{180\lambda}{B\sqrt{4\pi}} \; C \left[\left(\int_{-\infty}^{\infty} \int_{0}^{\pi} \sqrt{g(0)}\, \eta \, h_{\eta}(\eta)\delta(\alpha)\, d\alpha d\eta \right)^2 + \left(\int_{-\infty}^{\infty} \int_{0}^{\infty} \sqrt{g(\alpha)} f_2 h_{\alpha}(\alpha)\delta(\eta)\, d\alpha d\eta \right)^2 \right]^{1/2} . \tag{12}$$

Substituting (4), (5), and (11) into (12) and using the properties of a Rayleigh distribution function (see Appendix B), one readily obtains

$$\langle \tilde{v} \rangle = \frac{180\lambda}{B\sqrt{4\pi}} \; C \left[\bar{f}_1^2 + \bar{f}_2^2 \left(\frac{B^2}{4\ell n 2\sigma_2^2 + B^2} \right)^2 \right]^{1/2} . \tag{13}$$

Note that the mean of $\tilde{v}$ approaches $\frac{180\lambda}{B\sqrt{4\pi\rho}}\, C$ for wide beamwidth, i.e., $B^2 >> 4\ell n 2\sigma_2^2$. That is, the mean received signal is not degraded since its beamwidth is wide compared to the turbulence effects on angle of arrival.

The expression for $\tilde{v}^2$ is

$$\tilde{v}^2 = \frac{180^2\lambda^2}{B^2 4\pi} \; C^2 \left| g(0)\tilde{f}_1^2 + g(\alpha) f_2^2 + g(\alpha)\tilde{f}_1 f_2 \exp[-i(\tilde{\xi}_1 - \tilde{\xi}_2)] + g(\alpha)\tilde{f}_1 f_2 \exp[-i(\tilde{\xi}_2 - \tilde{\xi}_1)] \right| . \tag{14}$$

The second moment of $\tilde{v}$ is found by integrating Equation (14) and the pdf $h_1(\alpha,\eta)$ and pdf $h_2(\alpha,\eta)$ times variables containing $\tilde{f}_1$ and f_2, respectively. Integration on amplitude variable η is taken over $-\infty$ to ∞ and on angle variable α from 0 to π. Again, the phase integration on uniformly distributed random phase variables $\tilde{\xi}_1$ and $\tilde{\xi}_2$ over $-\pi/2$ to $\pi/2$ reduces the second moment to

$$\langle \tilde{v}^2 \rangle = \frac{180^2 \lambda^2}{B^2 4\pi} \; C^2 \int_{-\infty}^{\infty} \int_{0}^{\pi} [g(0) f_1^2 h_\eta(\eta)\delta(\alpha) + g(\alpha) f_2^2 h_\alpha(\alpha)\delta(\eta)] d\alpha d\eta \; . \tag{15}$$

It may then be shown that (Appendix C)

$$\langle \tilde{v}^2 \rangle = \frac{180^2 \lambda^2}{B^2 4\pi} \; C^2 \left[\sigma_1^2 + \bar{f}_1^2 + \bar{f}_2^2 \left(\frac{B^2}{8 \ell n 2 \sigma_2^2 + B^2} \right) \right] \; . \tag{16}$$

A gain reduction factor R may be defined in terms of $\langle \tilde{v} \rangle^2$ and $\langle \tilde{v} \rangle^2$ evaluated for $\sigma_2^2 = 0$ as

$$R = 10 \log_{10} \left. \frac{\langle \tilde{v} \rangle^2}{\langle \tilde{v} \rangle^2} \right|_{\sigma_2^2 = 0} \tag{17a}$$

$$R = 10 \log_{10} \frac{\bar{f}_1^2 + \bar{f}_2^2 \left(\frac{B^2}{4 \ell n 2 \sigma_2^2 + B^2} \right)^2}{\bar{f}_1^2 + \bar{f}_2^2} \; . \tag{17b}$$

This gain reduction represents available received mean signal power relative to the signal power available if angle of arrival effects were absent. A similar measure of received signal variance expressed in dB is

$$S^2 = 10 \log_{10} \frac{\langle \tilde{v}^2 \rangle - \langle \tilde{v} \rangle^2}{\langle \tilde{v} \rangle^2} \; , \tag{18}$$

$$S^2 = 10 \log_{10} \frac{\bar{f}_1^2 \sigma_1^2 + \frac{\bar{f}_2^2 B^2}{8 \ell n 2 \sigma_2^2 + B^2} - \bar{f}_2^2 \left(\frac{B^2}{4 \ell n 2 \sigma_2^2 + B^2} \right)^2}{\bar{f}_1^2 + \bar{f}_2^2 \left(\frac{B^2}{4 \ell n 2 \sigma_2^2 + B^2} \right)^2} \; . \tag{19}$$

This signal variance is a measure of fluctuating power in the received signal compared to the available received DC signal power.

The two statistical quantities which have now been defined, namely gain reduction, R, and signal variance, S^2, may be incorporated into distribution functions which are of the form used in link design. The long term time behavior of the received signal on a microwave link may be characterized by a fade distribution function. The turbulence induced effects with which we are dealing are long term average phenomena and hence are present at all times. A hypothetical low elevation angle fade distribution is presented in Figure 3. The abscissa is referenced to the signal level received in the absence of turbulence, i.e., including free space loss and gaseous absorption. The point at which the signal level is R dB is also the mean of the received signal; thus, one point on the fade distribution is established. The fade distribution for turbulence induced fluctuation is assumed to be log-normal, with mean and median being equal. The fade distributions resulting from the Ohio State University ATS-6 30 GHz beacon measurements (Ref. [30], pp. 72-75) indicate that this log-normal assumption is valid for elevation angles above approximately 2°. A similar observation was made concerning the 7.3 GHz fade distributions above 4° elevation angle observed by McCormick and Maynard (Ref. 35).

A fade distribution may now be produced using this assumption of linearity. Referring to Figure 3, it was noted that the point at which the received signal level is R dB represents the mean signal level. For a normal distribution, the mean is plotted at the 50% time abscissa exceeded point, indicated by ① in Figure 3. One standard deviation to the right of the mean on a normal distribution occurs at the 15.9% time abscissa exceeded level. It may be shown (Appendix E) that one standard deviation of received signal level, expressed in dB and denoted $\sigma_{V_{dB}}$, may be written in terms of the signal variance S^2. This point, $\sigma_{V_{dB}}$ to the right of R is denoted by ② in Figure 3. A

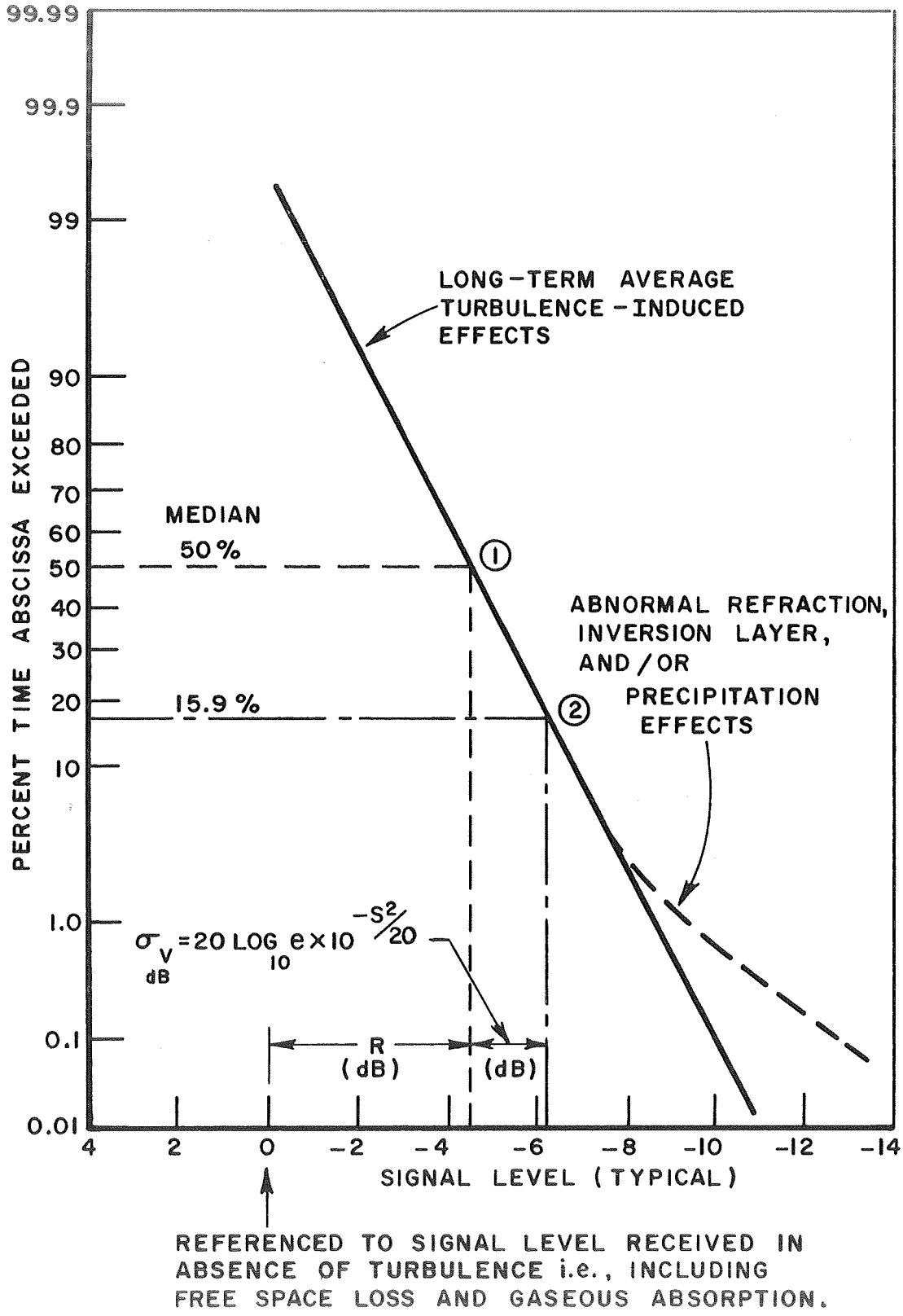

Figure 3. Fade distribution function.

straight line drawn between points ① and ② now approximately represents the fade distribution, referenced to the mean signal level in the absence of turbulence induced fluctuation. This distribution was based on small fluctuation arguments and should be employed as a lower bound when estimating a particular fade distribution.

Deviation of this fade distribution from the expected linear form will occur at small time percentages. Additional fading due to precipitation, abnormal refraction, or inversions in the atmosphere will cause greater fade depths for the small time percentages. However, the turbulence effects, which are always present, are still dominant for larger time percentages. For high elevation angles, i.e., short path lengths, S^2 will be very small and the line drawn through points ① and ② will be virtually vertical. However, the precipitation effects at the lower time percentages will still be present for short path length cases and will become the dominant feature of the fade distribution.

The expressions for R and S^2 will eventually be compared with measured data as a function of path length. But first, it is necessary to obtain expressions for σ_1^2 and σ_2^2.

CHAPTER III
EMPIRICAL CONSTANTS

Several measurements of angle of arrival variability of electromagnetic waves as they propagate through a turbulent atmosphere have been made. Ten experimental papers dealing with these measurements were examined and compared [18-27]. All results are for terrestrial microwave links operating at frequencies from 1 to 35 GHz over paths ranging in length from 5.5 to 80 km and located in various climatic regimes. In addition, angle of arrival statistics for an earth-space path from the Ohio State University CTS (Communications Technology Satellite) 11.7 GHz Beacon Experiment [28,29] are included.

Comparison between terrestrial and earth-space path propagation data may be made only if one assumes an equivalent atmospheric path length for the earth-space link. Although vertical gradients of temperature, pressure, water vapor density, and hence, refractivity exist in the atmosphere, one may replace this real atmosphere with a homogeneous atmosphere of some given height under standard temperature and pressure conditions for long term statistical purposes. It has been found, using amplitude scintillation measurements of the ATS-6 (Applications Technology Satellite - 6) 30 GHz beacon, than an equivalent atmospheric height of 6 km is sufficient for the prediction of long term time average scintillation behavior. Under this assumption, the CTS data taken at a 32° elevation angle traverses an atmospheric slant path over a curved earth equivalent to a 11.3 km terrestrial path.

The statistic to be compared from the several sources of data is the variance of the angle of arrival with respect to the mean direction of arrival, σ_2^2 expressed in dB below square degrees as

$$\sigma^2_{2_{dB}} = 10 \log_{10} \sigma_2^2 \quad . \tag{20}$$

The normalization with respect to one square degree is arbitrary but is necessitated by the fact that normalization to the mean angle of arrival has no physical significance. The papers in which these data appear

are not consistent in their definitions of variability. Hence, the following three conventions were assumed in an effort to make a meaningful comparison of the results

1) if variability was expressed as standard deviation σ_2 in parts per million (ppm) of wavelength (λ),

$$\sigma^2_{2_{dB}} = 10 \log_{10} \left[\text{Arctangent} \left(\frac{\sigma_2 \times \lambda}{\text{Receiver Separation}} \right) \right]^2 ; \quad (21)$$

2) if variability was expressed as a cumulative distribution function of relative angle of arrival, α, and plotted on Gaussian probability paper,

$$\sigma^2_{2_{dB}} = 10 \log_{10} \left[\frac{\alpha \text{ at 2.5 percentile} - \alpha \text{ at 97.5 percentile}}{4} \right]^2 ; \quad (22)$$

3) if variability was expressed as the observed maximum peak-to-peak excursion in α,

$$\sigma^2_{2_{dB}} = 10 \log_{10} \left[\frac{0.95 \times \text{max. peak-to-peak excursion of } \alpha}{4} \right] . \quad (23)$$

Table I summarizes the data and the method used to arrive at σ^2_2. The resulting angle of arrival variances are also shown in Figure 4. Obtaining σ^2_2 is quite subjective for many of the data sources, especially where limited measurements were presented. When a range of variances or probability density standard deviation limits were available, those limits were plotted as vertical lines through the data points in Figure 4.

The data of Table I suggest that variability increases proportionately with path length. Hence, the angle of arrival variance in dB σ^2_2 was plotted versus path length L in Figure 4 on a logarithmic scale. A first order regressive fit was then performed, resulting in:

$$\sigma^2_2 = 7.07 \times 10^{-6} \times L^{1.56} \ (\text{deg}^2) \quad (24)$$

with L expressed in kilometers. This relationship is shown as a solid line in Figure 3.

TABLE I

Fig. 4 Symbol	Data Source	Freq. (GHz)	Path Length (km)	σ_2^2 Average (dB below deg^2)	Method (1,2,3)
●	Deam & Fannin	9.35	5.5	-38.2	1
○	Herbstreit & Thompson	1.05	6.5	-37.0	3
□	Lees	35	10.5	-36.5	3
△	O.S.U. (equivalent Earth-Space path)	11.7	11.3	-32.8	2
‡	Lai-iun Lo	15.3	15.2	-40.75	3
■	Etcheverry et.al.	93	18.95	-31.4	3
◇	Lee & Waterman	35	28	-25.2	3
+	Akiyama et.al.	11,24	29	-27.7	2
+	Akiyama et.al.	11,24	33	-27.4	2
◆	Bell	11.0	55.4	-32	2
×	Janes et.al.	9.6	64.25	-20.4	1
×	Janes et.al.	34.5	64.25	-22.9	1
+	Akiyama et.al.	24	78.7	-21.62	2
*	Funakawa et.al.	12.6	80	-21.6	2

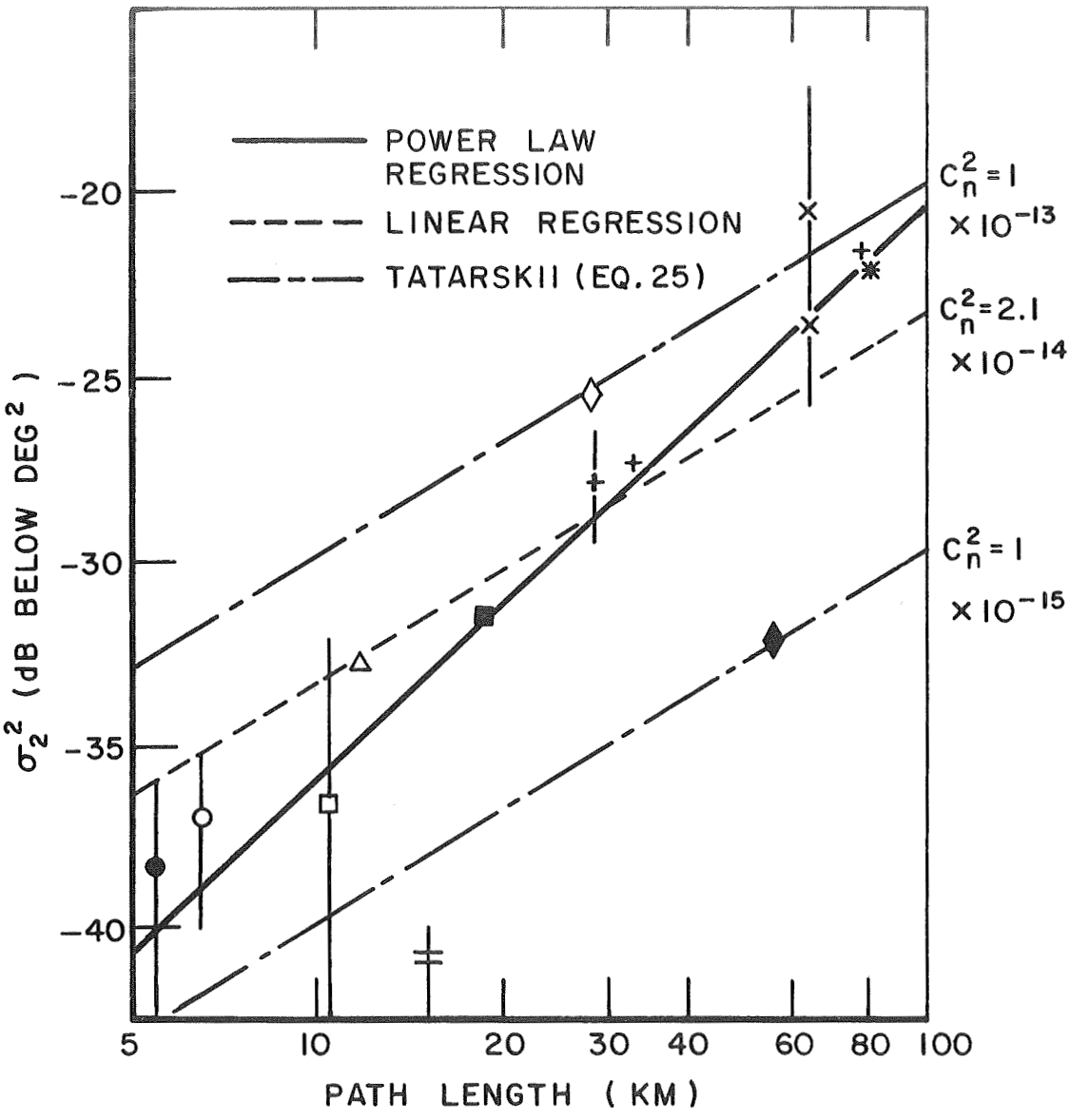

Figure 4. Measured angle of arrival data.

Theoretically, it can be easily shown [17] that angle of arrival variance should increase linearly with increasing path length in a turbulent atmosphere under the assumption that $L>>L_o$, i.e., the path length is much greater than the scale size of the largest turbulence-induced inhomogeneities present on the path. Also, angle of arrival variance σ_2^2 is mainly due to the large-scale components of the turbulence spectrum. Under these assumptions the turbulence theory of Tatarski leads to the following expression for σ_2^2

$$\sigma_2^2 = .0885\ C_n^2\ d^{-1/3}\ L \quad (\text{deg}^2) \tag{25}$$

where C_n is the refractive index structure constant. This theoretical expression is also plotted on Figure 4 for representative values of C_n^2, where d is aperture diameter and was taken as 1 m for the theoretical curve. The form of Equation (25) assumes that $d<<\sqrt{\lambda L}$, a valid assumption for millimeter and longer wavelengths at path lengths of several kilometers. Several uncertainties in the parameters of σ_2^2 may account for differences between the theoretical and the empirical regression curves. The angle of arrival variance σ_2^2 may vary $\pm$1.3 dB due to differences in aperture diameter d, $\pm$18.2 dB due to typical variations in the atmospheric structure constant C_n^2, or $\pm$4.6 dB due to the range of path elevations encountered in the experiments [31]. Additional differences may be due to inappropriateness of the plane wave assumption, especially for short path lengths or the requirement that $L>>L_o$, again, questionable for short path lengths.

The earth-space slant path data of Ohio State University falls within 2 dB of the regression line and, within the same limitations as the terrestrial data, agrees well with both the theoretical result as well as the other terrestrial measurements.

The empirical relationship (Equation (24)) which has just been presented obviates the problem of calculating σ_2^2 for our model in terms of a "representative" value for C_n^2, which may range over two orders of magnitude from time to time.

The last parameter to be determined is σ_1^2, the variance of the amplitude fluctuations. From Tatarskii [32], one finds that for weak fluctuations

$$\sigma_1^2 \sim C_n^2 \, K^{7/12} \, L^{11/6} \tag{26}$$

where K is the propagation constant.

We now have expressions for σ_1^2 and σ_2^2, both having unknown constant multipliers, and an unknown length, L_o, each of which must be empirically determined in order to predict long term average behavior of variance S^2 and gain reduction R. In the next section measured variance data were used to determine these constants.

Variance S^2 was measured as a function of elevation angle at 2 GHz with a 10 meter diameter antenna and at 30 GHz with a 5 meter diameter antenna [30]. A regressive power law fit was available for the data from elevation angles of 2° to 40° for the 2 GHz data and .5° to 40° for the 30 GHz data. These limits are such that the horizon did not lie within the 3 dB beamwidths of the antennas. Expressions for σ_1^2 and σ_2^2 in terms of the three unknown constants were used in the model of S^2 (Equation (19)). This expression was compared to the regression line from measured data at 2 and 30 GHz and the three constants were varied to obtain a regressive fit minimizing the following mean-square-error:

$$\underset{\begin{pmatrix} L_o \\ \sigma_1^2 \\ \sigma_2^2 \end{pmatrix}}{\text{Min}} \left\{ \frac{1}{200} \sum_{i=1}^{200} \left[S^2_{\substack{\text{measured} \\ 30\ \text{GHz}}} - S^2_{\substack{\text{model} \\ 30\ \text{GHz}}} \right] \Bigg|_{\substack{\text{elevation} \\ = ix\ .05^\circ}} \right.$$

$$\left. + \frac{1}{195} \sum_{i=5}^{200} \left[S^2_{\substack{\text{measured} \\ 2\ \text{GHz}}} - S^2_{\substack{\text{model} \\ 2\ \text{GHz}}} \right] \Bigg|_{\substack{\text{elevation} \\ = ix\ .05^\circ}} \right\} \tag{27}$$

Expressions (24) and (25) with both $L^{1.56}$ and $L^{1.0}$ dependence for σ_2^2 were employed in the regression defined above. The minimum error obtained for the $L^{1.56}$ dependence was approximately 40% less than that for the $L^{1.0}$ dependence case. Hence, although theory predicts linear behavior of angle of arrival variance as a function of path length, the $L^{1.56}$ form was used to compare the model to measured data and to obtain design curves. The final constants derived by the procedure outlined above which are used in the remainder of this work are:

$$L_o = 180\ (\text{km}) \tag{28a}$$

$$\sigma_1^2 = 2.6 \times 10^{-7}\ F^{7/12}\ L^{11/6} \tag{28b}$$

$$\sigma_2^2 = 5.67 \times 10^{-6}\ L^{1.56}\ d^{-1/3}\ (\text{deg}^2) \quad . \tag{28c}$$

Now that the model is complete, results from it will be compared with measured gain degradation and amplitude scintillation results in the next two sections.

CHAPTER IV
AMPLITUDE VARIANCE

The expression for received signal variance (Equation (19)) was compared as a function of elevation angle with data acquired from the 20 and 30 GHz ATS-6 satellite experiment as the satellite was moved from equatorial orbit at 94°W longitude toward 35°E longitude in 1975. The ground terminal at The Ohio State University, Columbus, Ohio employed a 4.5 m diameter parabolic, shared aperture antenna for both 20 and 30 GHz. The linear receiver output voltage was sampled at a data rate of 10 samples/sec and the variance, expressed in dB with respect to the DC power level for N samples, was calculated from

$$S^2 = 10 \log_{10} \left[\frac{\sum_{i=1}^{N} (v_i - \bar{v})^2}{N \bar{v}^2} \right] \quad ; \qquad n = 1024 \qquad (29)$$

where

$$\bar{v} = \frac{\sum_{i=1}^{N} v_i}{N} \quad . \qquad (30)$$

The apparent elevation angle of the satellite varied from 42° to almost 0° as it drifted eastward, and there were no optical obstructions along the propagation path. Time average variances, calculated according to Equation (29), were recorded for each elevation angle, consisting of clear air data periods of one to several hours in duration. Atmospheric path lengths were calculated assuming a spherical earth with a homogeneous atmosphere of height, h, and effective radius, R, taken as 4/3 the actual radius, or 8479 km, to account for standard refraction. The path length is then

$$L = [h^2 + 2hR + R^2 \sin^2 \theta]^{1/2} - R \sin \theta \qquad (31)$$

where θ is the elevation angle.

The data were fit in a minimum mean-square error sense to the form

$$S^2 = AL^B \tag{32}$$

using expression (31) for L and also regressively fit to determine the effective height, h. The results were

$$S_{20}^2 = 10^{-6.39}\, L^{2.29\pm.1} \tag{33}$$

$$S_{30}^2 = 10^{-6.2}\, L^{2.35\pm.1} \tag{34}$$

and $h = 5.9\pm1$ km . (35)

The model for received signal variance (Equation (19)) was then compared to these results using path lengths also calculated from Equation (31). This comparison of the calculated results and the regression fit to the experimental data is shown in Figure 5. Notice that the agreement is within a decibel or two over most of the range shown and for very low elevations the magnitude of the 30 GHz fluctuations is approaching the level of the DC component of the received power.

A second set of data was acquired in 1976 as the ATS-6 satellite was returned to 94°W. A 2 GHz linear receiver utilizing a 9.1 m diameter parabolic antenna was implemented and variance data were obtained according to Equations (29) and (30). The 20 GHz transmitter was not functioning during the 1976 transition, but the 30 GHz beacon was available. The comparison between the amplitude variance theoretical model and the 2 and 30 GHz experimental data is shown in Figure 6. The agreement between the theoretical model and the experimental results is better than that shown for the 1975 data.

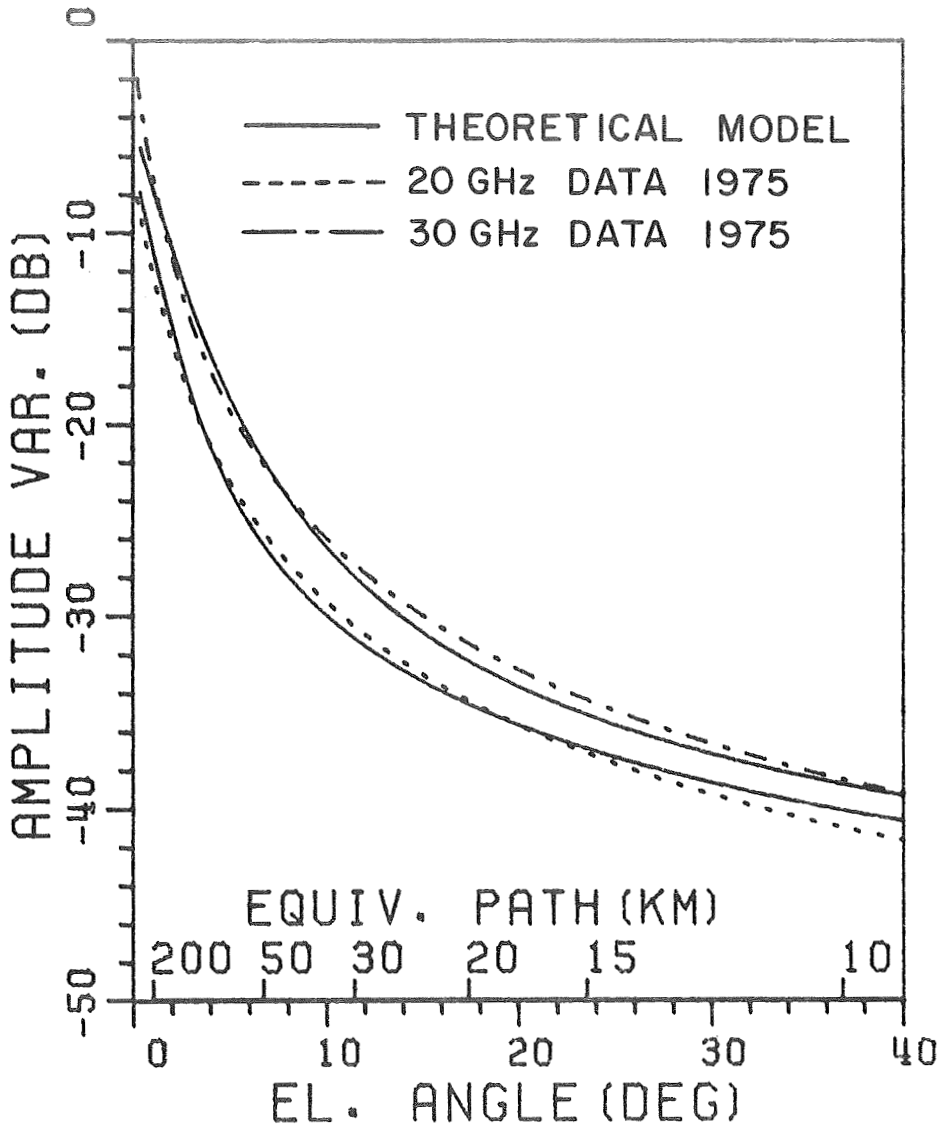

Figure 5. 1975 ATS-6 measured amplitude variance compared to theoretical model.

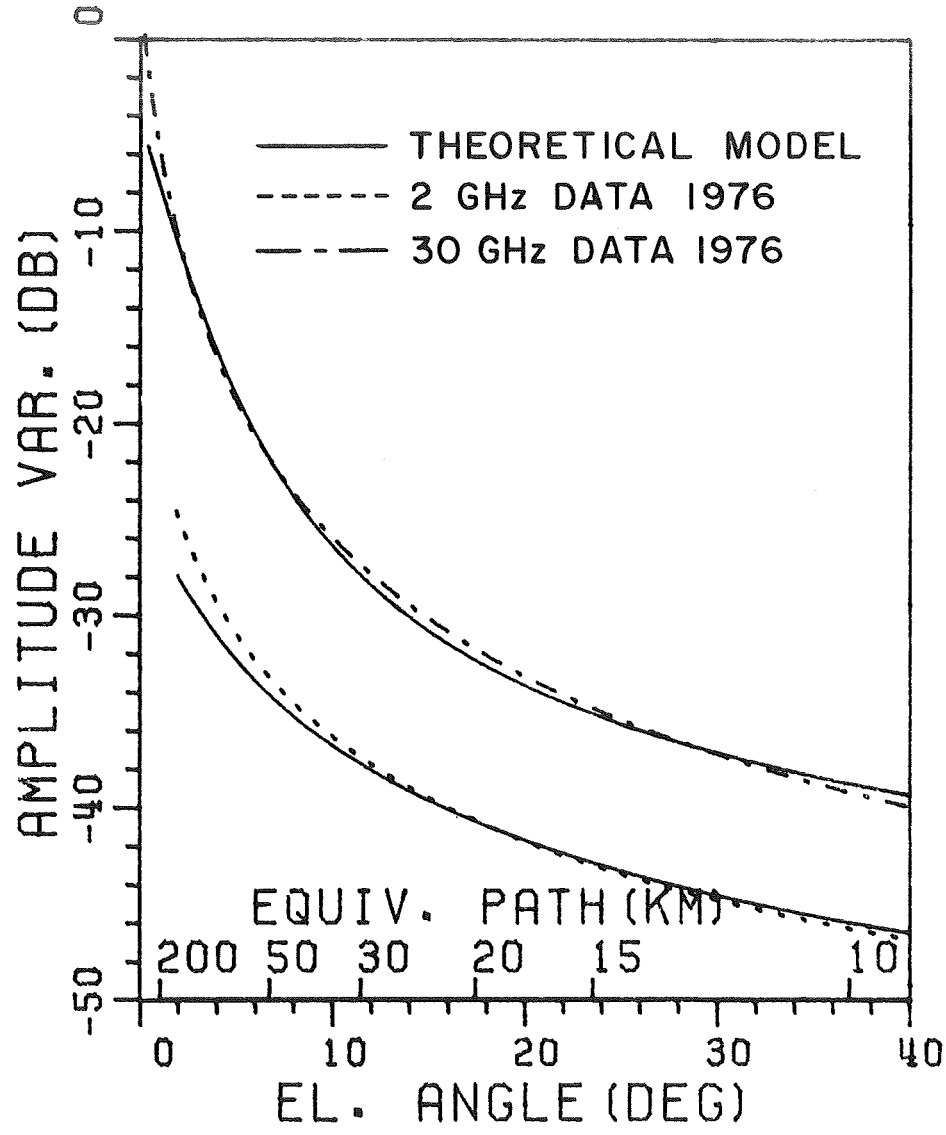

Figure 6. 1976 ATS-6 measured amplitude variance compared to theoretical model.

A final example compares the theoretical variance model with measurements of the IDCSP x-band beacon reported by R. K. Crane [33]. This experiment employed the 60 foot parabolic antenna at Westford, Massachusetts operating at a frequency of 7.3 GHz. Received power fluctuations were observed on angles from 0.5 to 10.0 degrees. Maximum and minimum limits were estimated from the data points presented in Reference [33], Figures 19 and 20, and plotted consistent with the definition of S^2. The mean of the limits, in dB, was also calculated. Figure 7 presents the means and limits of the measured data along with the variance predicted by the theoretical model. Again, the agreement is quite good.

The model (Equation (19)) for variance consists of amplitude and angle of arrival induced components, with each mechanism having greater or lesser importance depending on the path length, frequency, and beamwidth. To illustrate, consider Figure 8. The model for a 30 GHz signal and 4.6 in parabolic antenna is presented along with the constituent variance components due to amplitude only (i.e., $\sigma_2^2 = 0$ in Equation (19)) and angle of arrival only (i.e., $\sigma_1^2 = 0$ in Equation (19)). Note that the amplitude mechanism is most important at higher elevation angles and increases as elevation approaches zero. However, at about 11° the angle of arrival mechanism equals that of amplitude and then becomes dominant as the elevation angle decreases toward zero. Hence, amplitude scintillation resulting from angle of arrival effects for this case are relatively insignificant above 11°.

The manner in which the incident wave splits into angle and amplitude components is illustrated in Figure 9. The case plotted is for a 4.6 m diameter antenna at 30 GHz. The intensity has been normalized to the total power received at any position along the propagation path, i.e., atmospheric gas loss and free space path loss are not included.

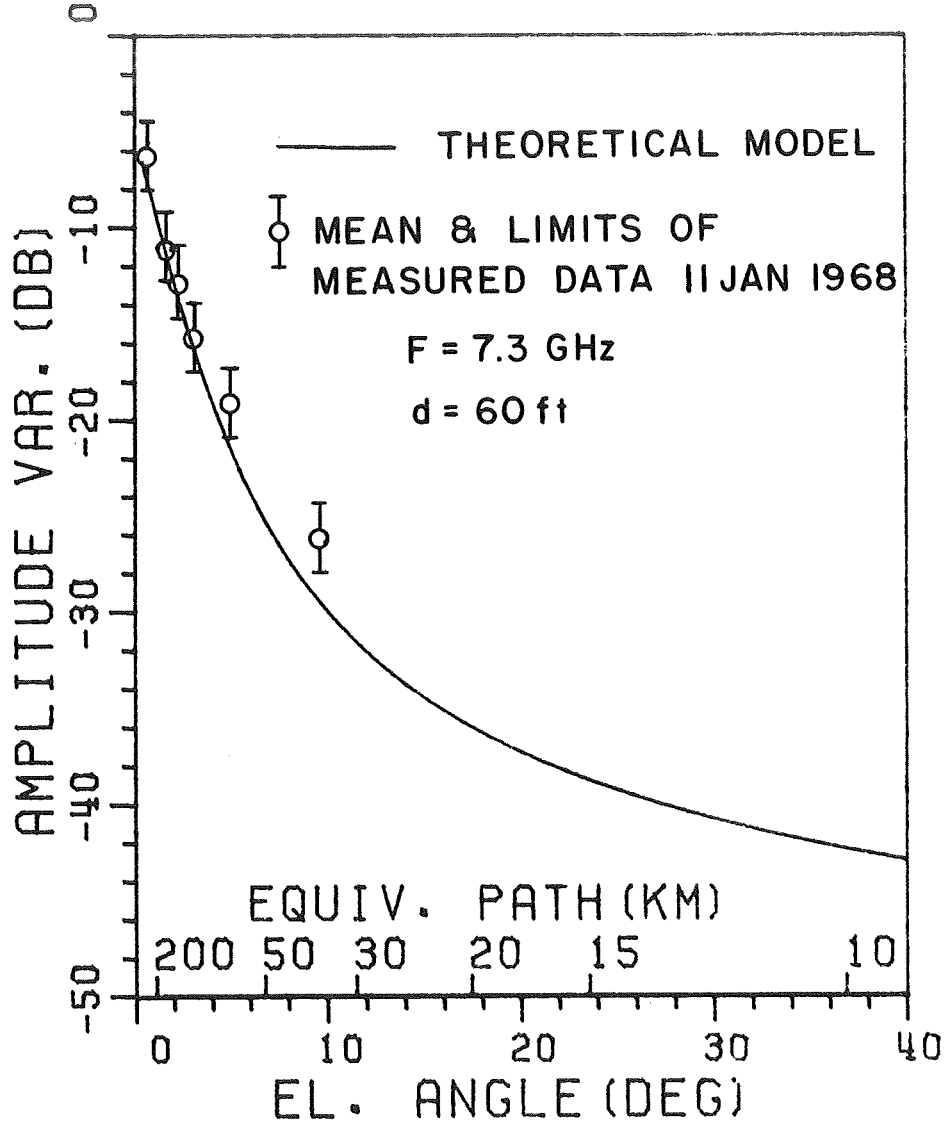

Figure 7. IDCSP X-band measured amplitude variance compared to theoretical model.

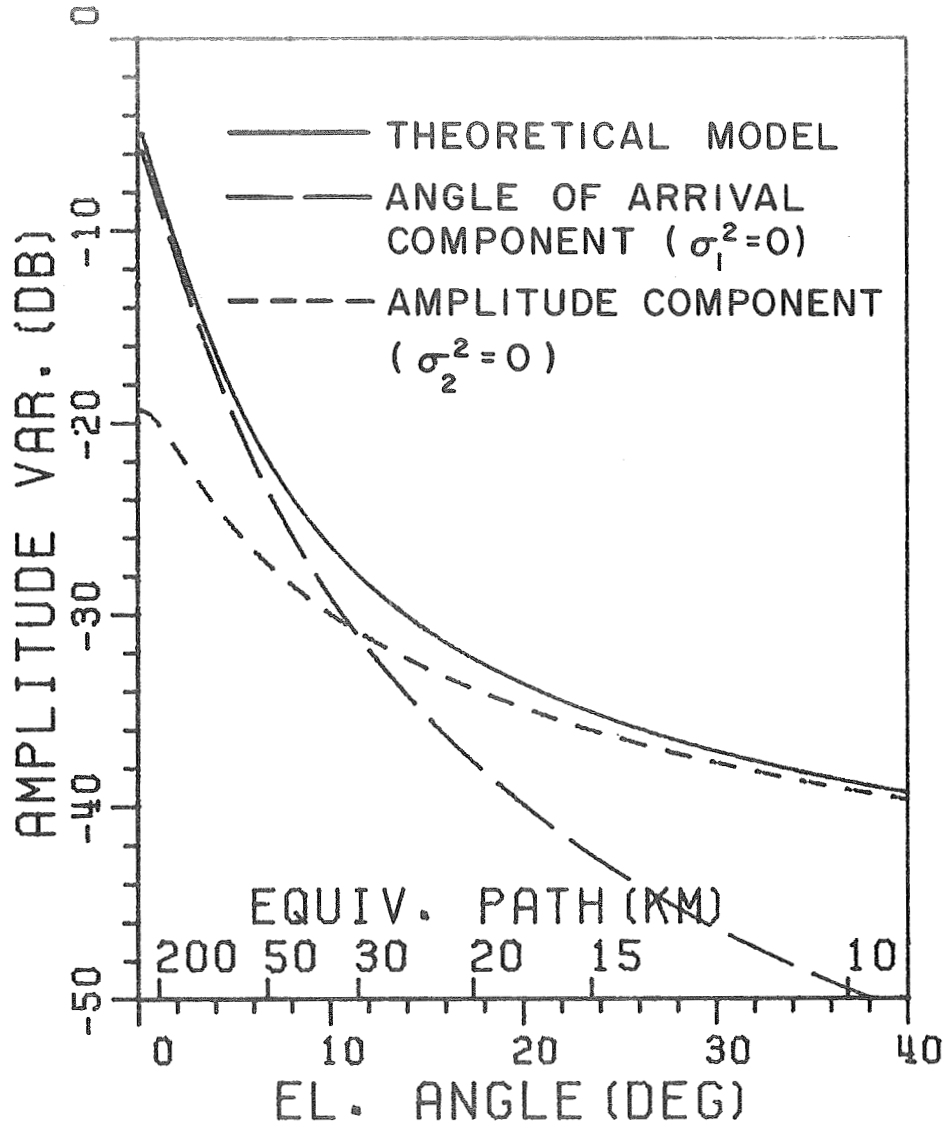

Figure 8. Amplitude and angle of arrival components of amplitude variance.

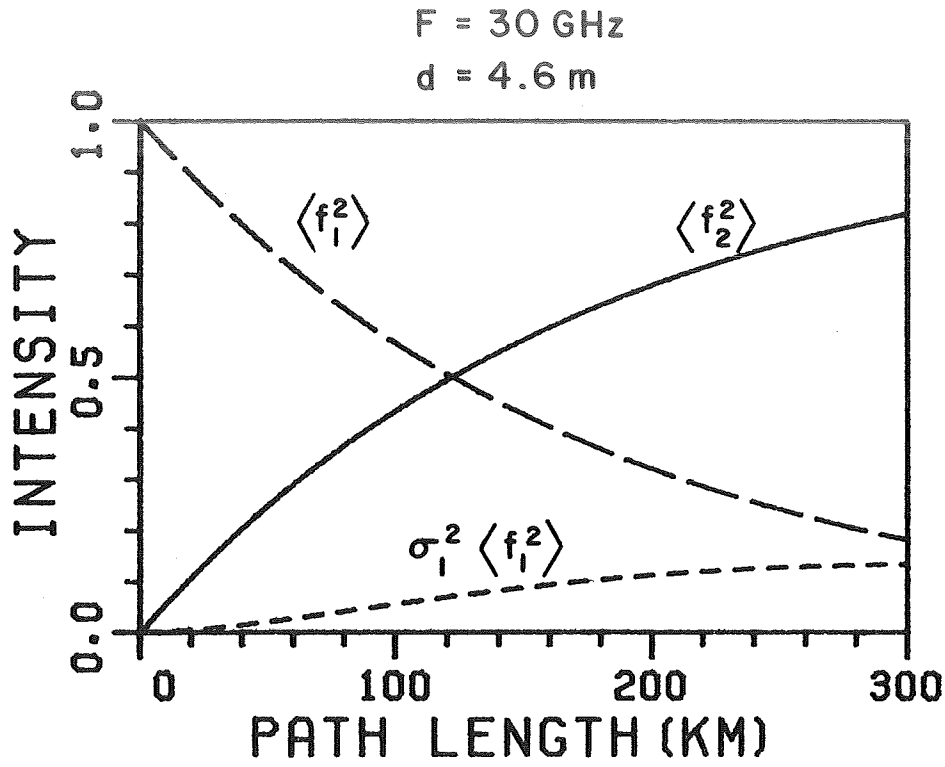

Figure 9. Amplitude and angle of arrival constituents of incident intensity.

The amplitude intensity, $\langle f_1^2 \rangle$, dominates for path lengths less than about 120 km in this case. For very long paths, $\langle f_1^2 \rangle$ becomes rather small and, in addition, power begins to transfer into the variance component $\sigma_1^2 \langle f_1^2 \rangle$. The angle component $\langle f_2^2 \rangle$ dominates for path lengths longer than 120 km thus implying the dominance of angle of arrival effects on received signal variance at low elevation angles.

The comparisons between the ATS-6 and IDCSP measurements and the theoretically predicted amplitude variances tend to justify the empirical results used to model amplitude variance σ_1^2 and angle of arrival variance σ_2^2. Although the method used to obtain average angle of arrival statistics as a function of path length involved subjectively reducing numerous reported forms of data to a single definition of

σ_2^2, the resulting theoretical model seems to predict long term time average amplitude fluctuation quite well. Daily variations of the atmospheric structure constant C_n^2 are averaged out in this type of modeling. However, the system designer may wish to account for the response of his communication link to the full range of expected C_n^2 variation which has been observed to be nominally ± 10 dB about the long term mean [34]. An example of such a maximum, minimum, and average received signal variance is presented in Figure 10, again, for a 4.6 m diameter antenna operating at 30 GHz. The maximum ± 10 dB range is present at higher elevation angles but shifts somewhat lower with respect to the average as the elevation angle decreases to zero. Similar behavior is expected for other combinations of frequency and aperture size.

The frequency dependence of the amplitude variance for a fixed aperture size is shown in Figure 11. This family of design curves presents long term time average received signal variances for a 4.6 m diameter parabola with frequency ranging from 1 to 100 GHz. The comparisons between theoretical and experimental results presented above indicate that the model is acceptable for frequencies between 2 and 30 GHz. The curve for 100 GHz is included only as an indication of the degree of amplitude scintillation to be expected if extrapolation using this model is warranted. This model establishes a lower bound on the expected amplitude scintillation at 100 GHz because refractive layers, abnormal focusing, or non-negligible scattering at this frequency, and consequently very narrow beamwidth (.04°) for a 4.6 m aperture, will enhance the scintillation.

Comparison of measured and calculated variance lends a measure of credibility to the model, at least from 2 to 30 GHz. The second quantity which the theoretical model predicts, namely gain degradation, will now be compared with experimental data as a function of elevation angle.

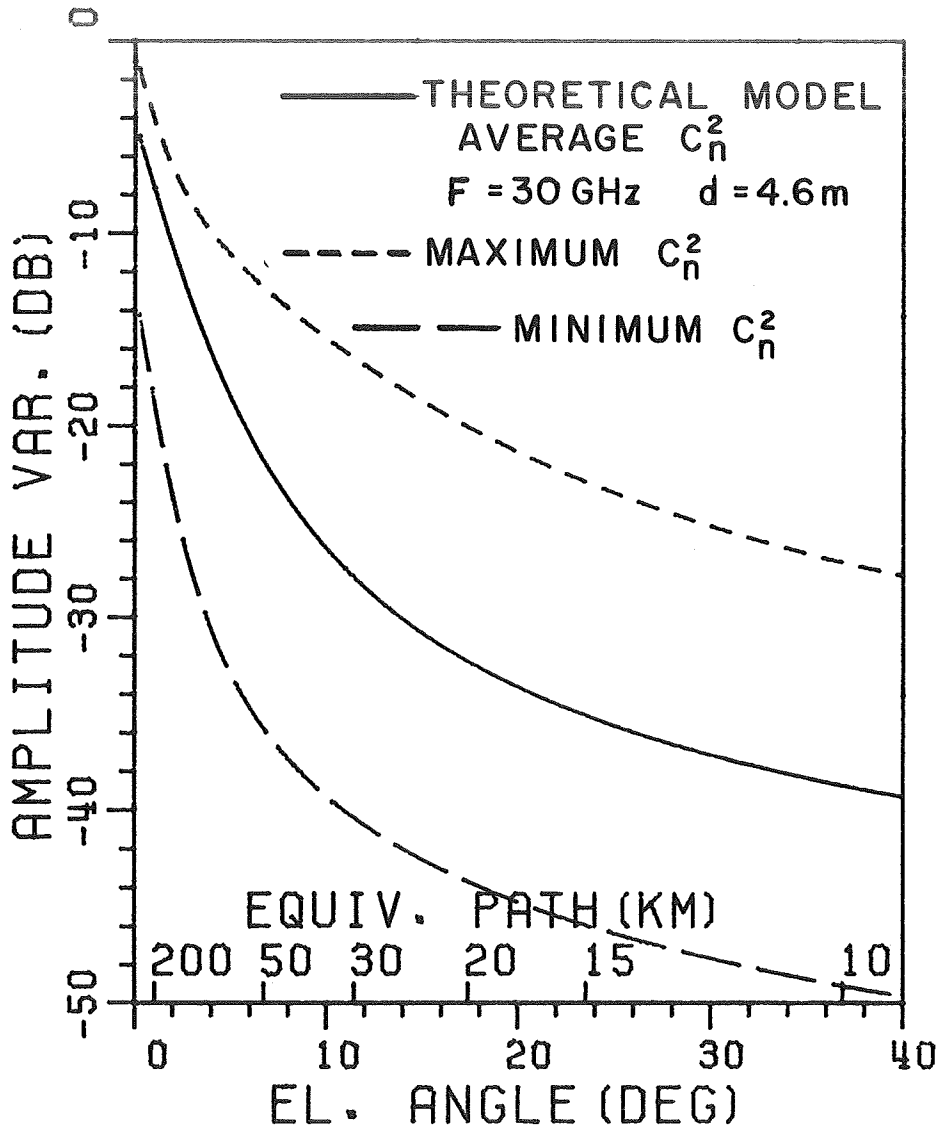

Figure 10. Maximum and minimum effects of C_n^2 on amplitude variance.

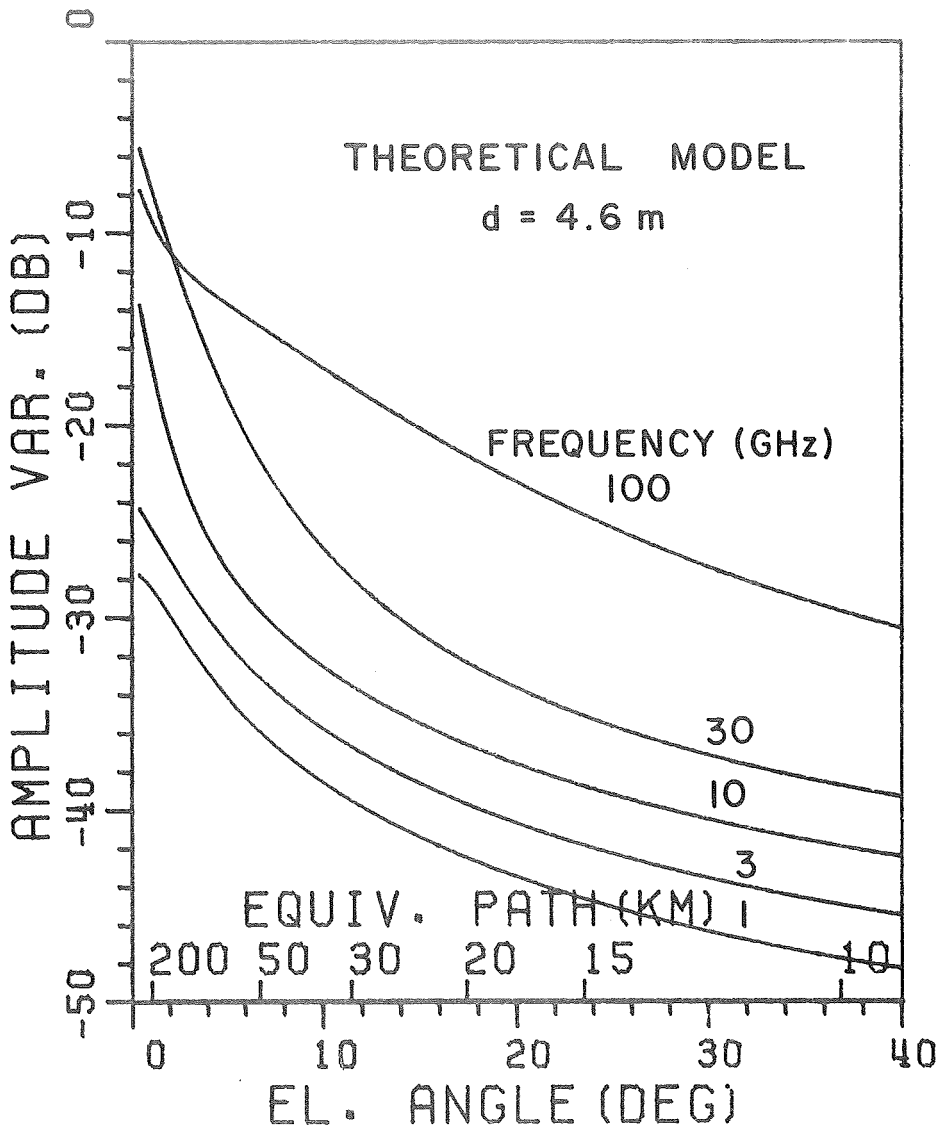

Figure 11. Frequency dependence of amplitude variance.

CHAPTER V
GAIN DEGRADATION

The expression for long term time average received signal level (Equation (17)) as a function of elevation angle was also compared with measured satellite data. As the ATS-6 satellite (2 and 30 GHz beacons) was moved from equatorial orbit at 35°E longitude toward 94°W longitude, average received signal level was recorded and plotted as a function of elevation angle from 0° to 40° [30]. A 4.6 m diameter Cassegrainian antenna was employed at 30 GHz and a 9.1 m diameter focal point feed antenna was utilized at 2 GHz. In addition, median signal level as a function of elevation angle is available from measurements made by McCormick and Maynard at the Communications Research Center in Ottawa, Canada using the US TACSATCOM-1 7.3 GHz beacon [35]. The median signal level was received with a .3° beamwidth antenna as the satellite drifted westward, with elevation angle decreasing from 6° to 0.5° over a period of 23 days. The data from Reference [35], Figures 1 and 2, were presented as a series of distributions of received signal level as a function of one degree increments of elevation angle. The means were assumed to be the signal levels at the 50% time ordinate and these means were associated with the elevation angles at the center of the one degree increments.

The theoretical model was used to predict mean signal level degradation due to atmospheric fluctuation as a function of elevation. This gain degradation was combined with atmospheric gas loss calculated for a 6 km equivalent height homogeneous atmosphere at standard temperatuare and pressure and plotted in dB relative to the received signal level at 90° elevation angle. Predicted curves are presented in Figure 12 for 2, 7.3 and 30 GHz for antenna beamwidths of 1.8°, 0.3° and 0.15°, respectively, along with measured mean signal levels from the ATS-6 and TACSATCOM experiments. The agreement is quite good, verifying that the theoretical model adequately predicts long term time average gain degradation as well as amplitude variance.

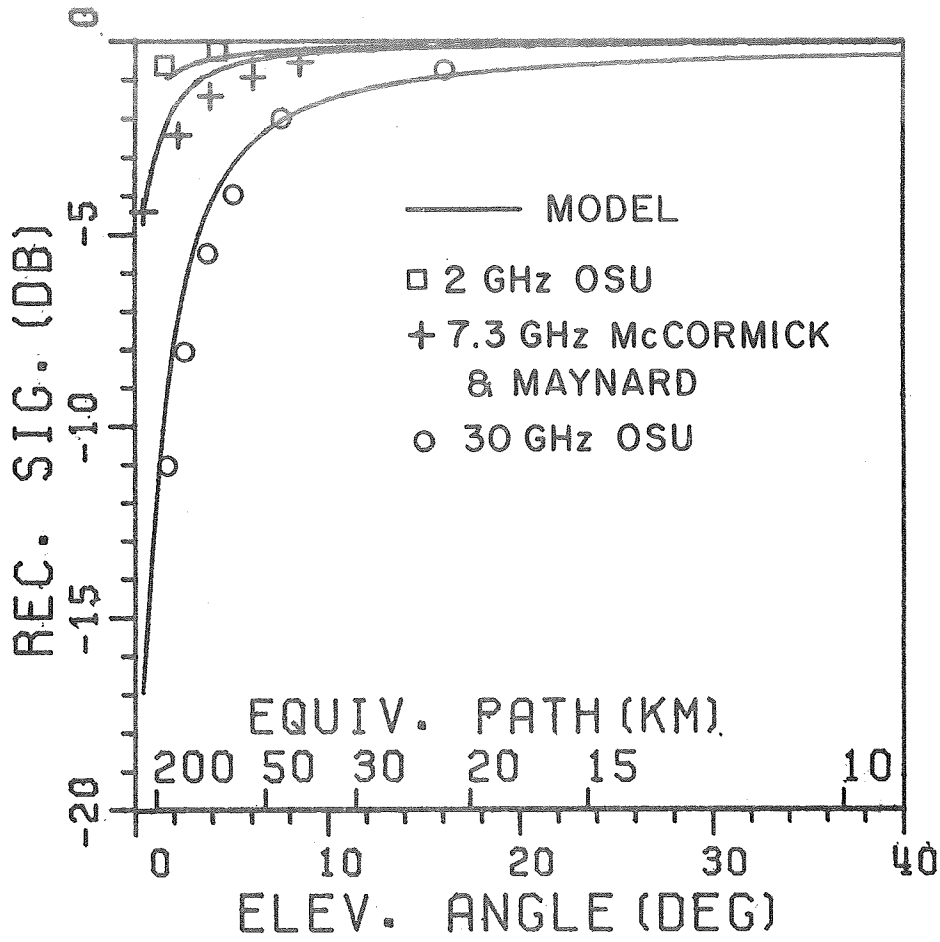

Figure 12. Measured received signal level compared to theoretical model.

An additional plot, Figure 13, presents only the gain degradation component due to atmospheric turbulence, i.e., excluding atmospheric gas loss. Compared to Figure 12, gas loss is certainly the major contribution to signal loss at low elevation angles, but gain degradation due to atmospheric turbulence is also significant, especially for the narrow beamwidth, millimeter wave-length case. It may be shown that the most significant parameter in the fluctuation degradation component

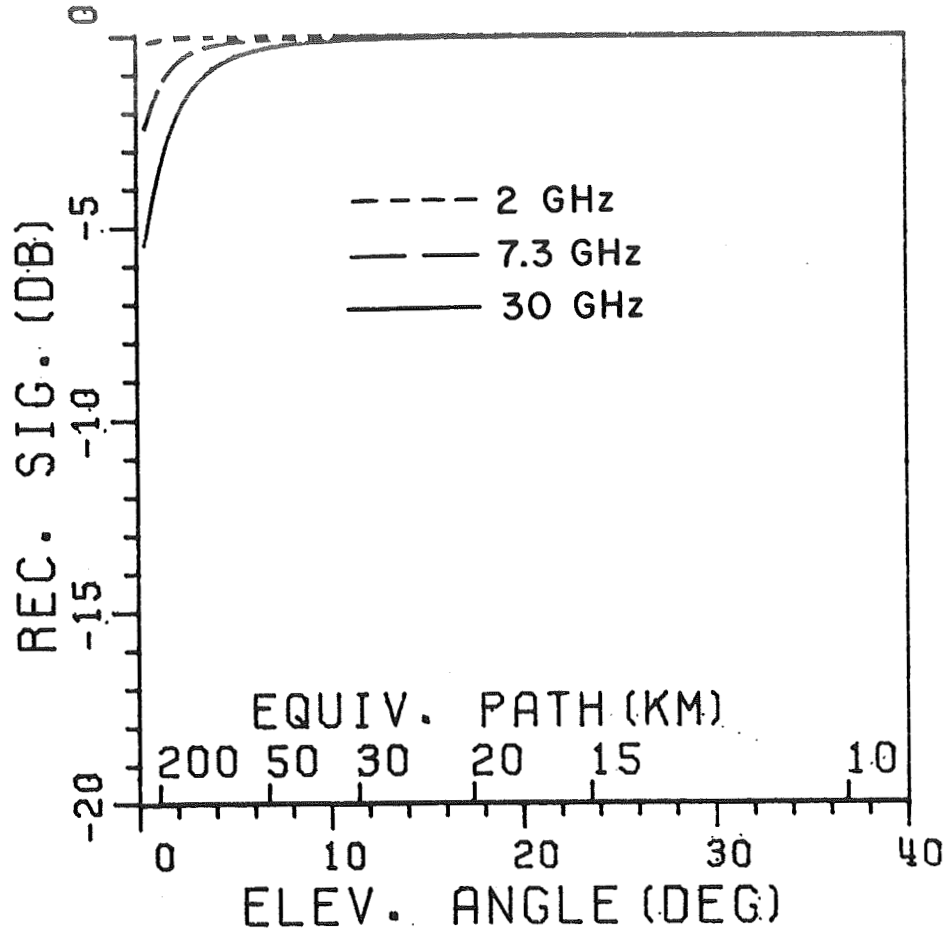

Figure 13. Gain degradation component of received signal level.

is beamwidth. To illustrate, consider Figure 14. Gain degradation, due to atmospheric fluctuation only, as a function of elevation angle is presented for several beamwidths at a frequency of 30 GHz. Less than 1 dB of degradation occurs down to elevation angles of about 10° (34.2 km equivalent path length) even for 0.05° beamwidth. Hence, the long term time average gain degradation is relatively minor for path lengths less than 34 km or elevation angles above 10°. To facilitate an estimation of expected gain degradation in communication link design, several design curves will now be presented.

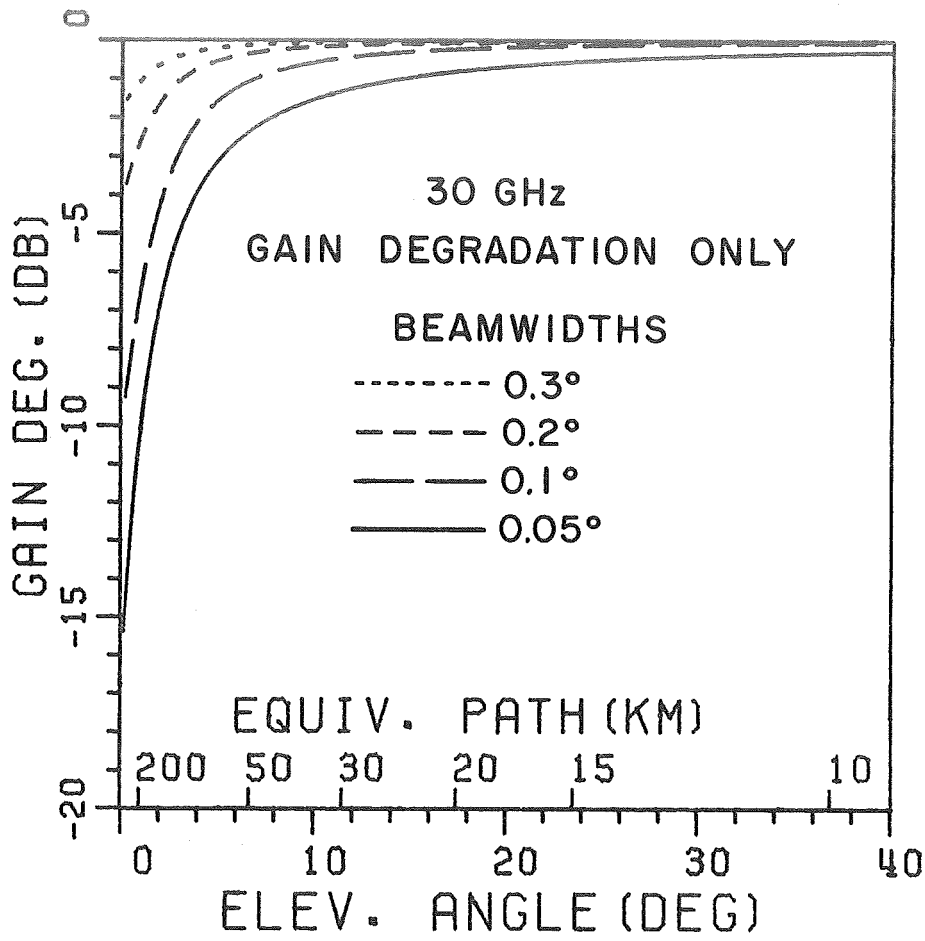

Figure 14. Beamwidth dependence of gain degradation.

Realized gain as a function of antenna beamwidth or equivalent aperture diameter at 30 GHz is plotted in Figure 15. All equivalent aperture diameters, given a particular beamwidth and frequency, will be presented for an antenna efficiency of 0.6. The curve representing zero path length L is simply the common gain approximation

$$G = \frac{41253}{B^2} \quad . \tag{36}$$

Realized gain curves for path lengths of 50 to 300 km are plotted using the theoretical model. Equivalent earth-space path elevation angles assuming a 6.0 km height homogeneous atmosphere are presented in parenthesis.

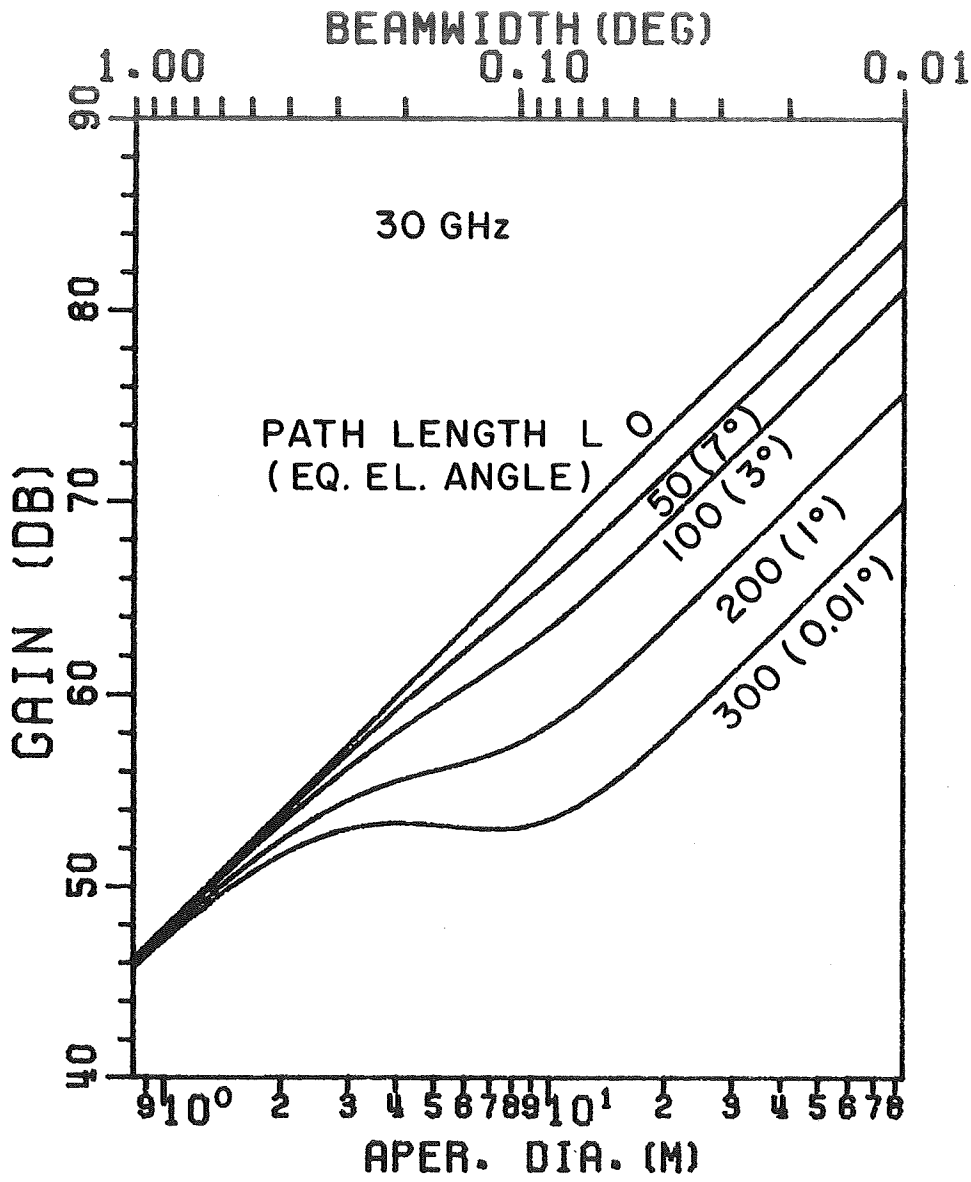

Figure 15. Path length dependence of gain degradation.

Notice that gain degradation due to turbulence induced fluctuation is negligible for beamwidths wider than about 0.7° for all path lengths. Degradation effects then gradually increase as beamwidth narrows from 0.7° to 0.05° and at any particular beamwidth are approximately directly proportional, in dB, to path length. As beamwidth narrows beyond 0.05°, a saturation effect occurs and the degradation becomes constant for any one path length. An elementary explanation is that for any path length, as beamwidth becomes extremely small, the angle of arrival (incoherent) component of the incident wavefront, $\langle f_2^2 \rangle$, contributes little to the power received by the aperture since this angle of arrival component has negligible probability of being within the 3 dB beamwidth of the antenna. However, the amplitude component (coherent and on-axis) remains constant and the power which the aperture receives due to this component is only a function of path length and not aperture size.

The frequency dependence of gain degradation is illustrated for several beamwidths at 3 and 30 GHz in Figure 16. For the longest path length, 300 km and for beamwidths wider than 0.2°, gain degradation is virtually independent of frequency. At the narrowest beamwidth, .05°, the degradation differs by approximately 1 dB. Hence, the turbulence induced degradation effect is quite insensitive to frequency, as opposed to the strong dependence it has on beamwidth.

The data of Figure 16 may be quite useful to the design engineer employing large apertures at millimeter wavelengths. For example, after considering atmospheric gas loss at a particular frequency on a low elevation earth-space path for a 0.2° beamwidth antenna, the engineer may decide that he must double the aperture diameter (halve beamwidth) in order to attain a particular system margin. However, looking at Figure 16, if the equivalent path length were 200 km the link design should include a 4 dB average gain loss at .2° beamwidth and still another 4 dB when going to .1°. In some cases, it might be

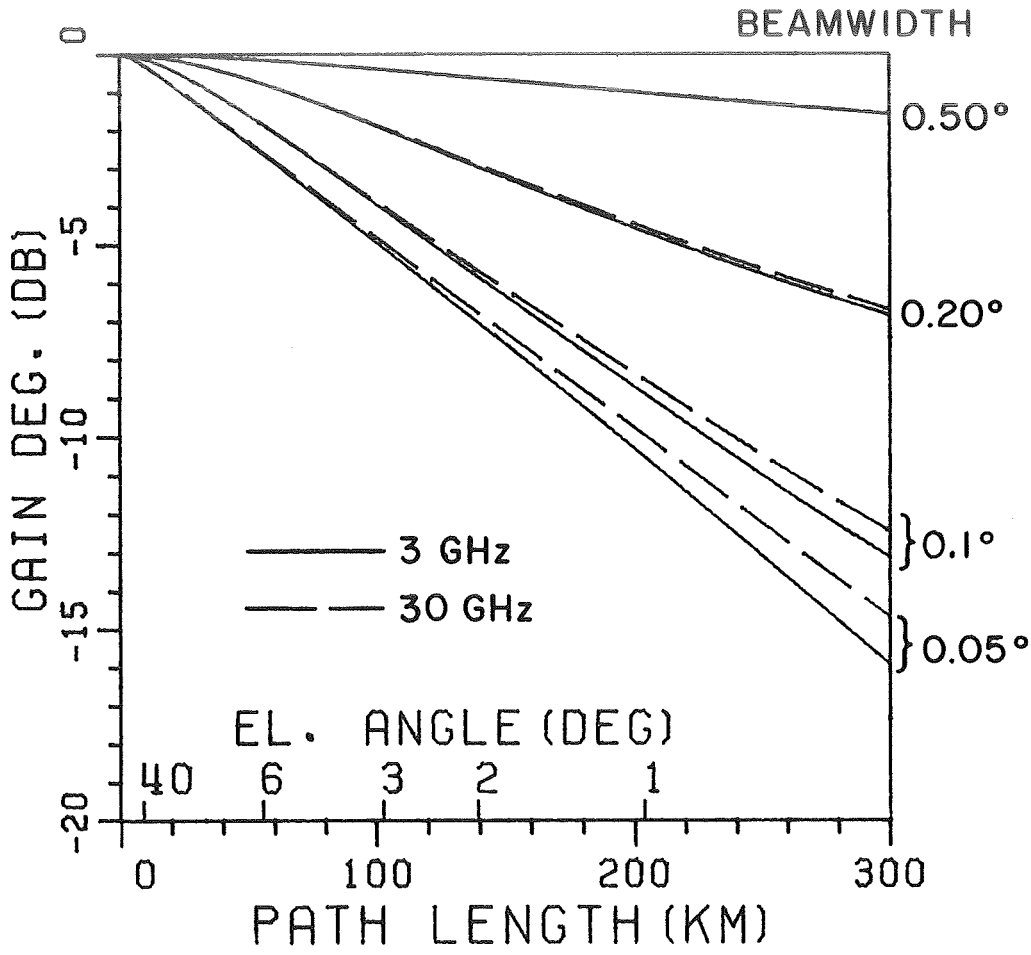

Figure 16. Frequency dependence of gain degradation.

more economical to employ self-phased array antennas having elements of relatively wide beamwidth (say .5°, referring to Figure 16) such that adequate gain is achieved by adding elements whose individual power patterns are wide enough so that average gain degradation and amplitude variations due to turbulence are negligible.

CHAPTER VI
CONCLUSION

A model including the two coupled mechanisms of microwave angle of arrival fluctuation and amplitude scintillation due to tropospheric turbulence appears to be adequate for the prediction of long term time average received signal levels and amplitude fluctuations on earth-space and terrestrial propagation paths. The utility of an equivalent 6 km high homogeneous atmosphere and a long term expected value for the atmospheric structure constant has been emphasized when deriving the empirical constants necessary to produce design curves from the model. The model does not address orographic or marine effects, but its ability to predict observed data from Massachusetts, Ohio and Ontario indicates that long term statistics of atmospheric turbulence may not be strongly dependent upon the particular location or climatic regime.

Design curves based on this model indicate that both received signal level reduction and amplitude scintillation due to tropospheric turbulence are most apparent at narrow beamwidths. In the design of a long path length terrestrial microwave link or a low elevation angle earth-space link, the engineer must consider gain loss and amplitude scintillation due to tropospheric turbulence if he wishes to use large aperture, narrow beamwidth antennas. In cases where the angle of arrival mechanism dominates, it may be advantageous to utilize self-phased arrays to circumvent the gain degradation and scintillation introduced by this mechanism. The theoretical model, when properly applied, will indicate when such measures are necessary.

REFERENCES

[1] V. I. Tatarski, Wave Propagation in a Turbulent Medium, translated from Russian by R. A. Silverman, 285 pages, McGraw-Hill, New York, 1961.

[2] V. I. Tatarski, The Effects of the Turbulent Atmosphere on Wave Propagation, translated from Russian by Israel Program for Scientific Translations, Rep. N 72-18163, 472 pages, National Technical Information Service, Springfield, Virginia.

[3] R. W. Schmeltzer, "Means, Variances, and Covariances for Laser Beam Propagation Through a Random Medium," Quart. Appl. Math., Vol. 24, 1967, pp. 339-354.

[4] R. W. Lee and J. C. Harp, "Weak Scattering in Random Media, with Applications to Remote Probing," Proc. of the IEEE, Vol. 57, No. 4, April 1969, pp. 375-406.

[5] S. F. Clifford, "Temporal Frequency Spectra for a Spherical Wave Propagating Through Atmospheric Turbulence," J. Opt. Soc. Amer., Vol. 61, No. 10, 1971, pp. 1285-1292.

[6] A. Ishimaru, "Temporal Frequency Spectra of Multifrequency Waves in a Turbulent Atmosphere," IEEE Trans. Ant. and Prop., AP-2(1), 1972, pp. 10-19.

[7] P. A. Mandics, R. W. Lee and A. T. Waterman, Jr., "Spectra of Short-Term Fluctuations of Line-of-Sight Signals: Electromagnetic and Acoustic," Radio Science, Vol. 8, No. 3, March 1973, pp. 185-207.

[8] M. E. Gracheva and A. S. Gurvich, "Strong Fluctuations in the Intensity of Light Propagated Through the Atmosphere Close to the Earth," Izev. Vyssh. Ucheb. Zaved. Radiofiz., Vol. 8, 1965, pp. 717-724.

[9] L. A. Chernov, Wave Propagation in a Random Medium, McGraw-Hill, New York, 1960.

[10] R. S. Lawrence and Strohbehn, "A Survey of Clear Air Propagation Effects Relevant to Optical Communications," Proc. IEEE, Vol. 58, October 1970, pp. 1523-1545.

[11] R. L. Fante, "Electromagnetic Beam Propagation in Turbulent Media," Proc. IEEE, Vol. 63, 1975, pp. 1669-1692.

[12] Y. Baraban, et. al., "Status of the Theory of Propagation of Waves in a Randomly Inhomogeneous Medium," Sov. Phys.-Usp., Vol. 13, 1971, pp. 551-580.

[13] A. Ishimaru, "Theory and Application of Wave Propagation and Scattering in Random Media," Proc. IEEE, Vol. 65, No. 7, July 1977, pp. 1030-1061.

[14] V. I. Tatarski, The Effects of the Turbulent Atmosphere on Wave Propagation, translated from Russian by Israel Program for Scientific Translations, Rep. N 72-18163, National Technical Information Service, Springfield, Virginia, p. 293.

[15] R. W. Lee et. al., Op. Cit., p. 390.

[16] A. Papoulis, Probability, Random Variables, and Stochastic Processes, McGraw-Hill Book Co., 1965, pp. 194-195.

[17] V. I. Tatarski, The Effects of the Turbulent Atmosphere on Wave Propagation, translated from Russian by Israel Program for Scientific Translations, Rep. N 72-18163, National Technical Information Service, Springfield, Virginia, pp. 288-289.

[18] A. P. Deam, and B. M. Fannin, "Phase Difference Variations in 9350-Megacycle Radio Signals Arriving at Spaced Antennas," Proc. IRE, 43(10), p. 1402, 1955.

[19] J. W. Herbstreit, and M. C. Thompson, "Measurements of the Phase of Radio Waves Received over Transmission Paths with Electrical Lengths Varying as a Result of Atmospheric Turbulence," Proc. IRE, 43(10), p. 1391, 1955.

[20] M. L. Lees, "High Resolution Measurement of Microwave Refraction on Short Tropospheric PAths," IEEE Trans. Ant. & Prop., Vol. AP-20, March 1972, pp. 176-181.

[21] R. W. Lee and A. T. Waterman, Jr., "A Large Antenna Array for Millimeter Wave Propagation Studies," Proc. IEEE, Vol. 54, No. 4, April 1966, pp. 454-458.

[22] T. Akiyama, S. Agyagi and H. Yoshida, "Variability of the Angle of Arrival of Microwaves," Electronics and Communications in Japan, Vol. 50, Feburary 1967, pp. 60-67.

[23] H. B. Janes, M. C. Thompson, Jr., D. Smith, and A. W. Kirkpatrick, "Comparison of Simultaneous Line-of-Sight Signals at 9.6 and 34.5 GHz.," IEEE Trans. Ant. and Prop., Vol. AP-18, No. 4, July 1970, pp. 447-451.

[24] K. Funakawa, T. Kido, K. Kitamura, Y. Otsu, T. Katto and M. Uratsuka, "Propagational Experiments of 13 GHz and 35 GHz Over the Path 80 km, Tsukuba to Kokubunji," Journal of the Radio Research Laboratories, Vol. 14, No. 76, November 1967, pp. 249-265.

[25] Lai-iun Lo, "Propagation Measurements of Amplitude and Phase Fading on a Line-of-Sight Path at 2 cm," Technical Report No. 70-1, Air Force Avionics Laboratories, Wright-Patterson Air Force Base, Dayton, Ohio, 31 March 1970.

[26] R. D. Etcheverry, G. R. Heidbreder, W. A. Johnson and H. J. Wintroub, "Measurements of Spatial Coherence in 3.2-mm Horizontal Transmission," Air Force Report No. SSD-TR-67-31, Aerospace Corp., January 1967.

[27] J. Bell, "Propagation Measurements at 3.6 and 11 Gc/s Over a Line-of-Sight Radio Path," The IEE Proceedings in Electronics, Vol. 114, No. 5, May 1967, pp. 545-547.

[28] D. M. Theobold and D. B. Hodge, "The OSU Self-Phased Array for Propagation Measurements Using the 11.7 GHz CTS Beacon," Report 4299-1, November 1976, The Ohio State University Electro-Science Laboratory, Department of Electrical Engineering; prepared under Contract NAS5-22575 for NASA-Goddard Space Flight Center. (NASA-CR-152519) (N77-24334)

[29] D. B. Hodge and D. M. Theobold, "OSU Participation in the CTS Communications Link Characterization Experiment," (Final) Report 4299-2, December 1976, The Ohio State University Electro-Science Laboratory, Department of Electrical Engineering; prepared under Contract NAS5-22575 for NASA-Goddard Space Flight Center. (NASA-CR-152534) (N77-25371)

[30] D. Devasirvatham and D. B. Hodge, "Amplitude Scintillations on Earth Space Propagation Paths at 2 and 30 GHz," Report 4299-4, March 1976, The Ohio State University ElectroScience Laboratory, Department of Electrical Engineering; prepared under Contract NAS5-22575 for NASA-Goddard Space Flight Center.

[31] W. D. Brown, "A Model for the Refractive-Index Structure Constant at Microwave Frequencies," Internal Report SAND 76-0593, Sandia Laboratories, Albequerque, N.M., February 1977, p. 24.

[32] V. I. Tatarski, Op. Cit., pp. 326-327.

[33] R. K. Crane, "Propagation Phenomena Affecting Satellite Communication Systems Operating in the Centimeter and Millimeter Wavelength Bands," Proc. of IEEE, Vol. 59, No. 2, February 1971, pp. 173-188.

[34] V. I. Tatarski, Op. Cit., p. 151.

[35] K. S. McCormick and L. A. Maynard, "Measurements of S.H.F. Tropospheric Fading Along Earth-Space Paths at Low Elevation Angles," Electronics Letters, Vol. 8, No. 10.

[36] A. Papoulis, Probability, Random Variables, and Stochastic Processes, McGraw-Hill, New York, 1965, pp. 151-152.

APPENDIX A
LINK PARAMETERS

- The magnitude of the electric field component $|E_i|$ incident on an antenna aperture is given in the text in Equation (1).

- The power density at the receiver, P_r, in terms of the medium impedance, Z_o, may be expressed as

$$P_r = \frac{1}{2} C^2/Z_o$$

where C is the magnitude of the incident electric field intensity.

- The following parameters are required to characterize the communications link:

1. P_t transmitted power in watts
2. G_t transmit antenna power gain
3. L_{fs} free space loss = $16\pi^2L^2/\lambda^2$ for a path length L at wavelength λ
4. L_{atm} atmospheric gas loss (water vapor & oxygen)

- $A_e = \lambda^2 G(\alpha)/4\pi$ is the effective aperture area of the receiving antenna with parameters

1. λ wavelength
2. $G(\alpha)$ antenna power gain (a function of angle α).

Alternatively, the antenna gain may be expressed in terms of a pattern factor, $g(\alpha)$, defined by:

$$G(\alpha) = \frac{4}{\pi} \times \frac{180^2}{B^2} \; g(\alpha),$$

where B is the antenna half-power beamwidth expressed in degrees. A representative Gaussian antenna pattern factor (Equation (11)) may be expressed as

$$g(\alpha) = \exp \left[-\frac{\alpha^2 4 \ell n 2}{B^2} \right]$$

$$g_{dB}(\alpha) = -3 \left[\frac{\alpha^2}{(\frac{B}{2})^2} \right] .$$

Gain degradation, R, as discussed in the text, results from angle of arrival fluctuation and is a function of frequency, path length, and aperture size.

All of the parameters defined above may be written concisely in terms of decibels to describe received power in terms of transmitted power, transmit antenna gain, free space loss, atmospheric gas loss, gain degradation, and effective aperture area as:

$$P_{r_{dBW}} = P_{t_{dBW}} + G_{t_{dB}} - L_{fs_{dB}} - L_{atm_{dB}} - R_{dB} + A_{e_{dB}} .$$

APPENDIX B
FIRST MOMENT OF $\tilde{v}$

The receiver output voltage may be written:

$$\tilde{v} = \frac{\lambda}{\sqrt{4\pi}} \; C\left|\sqrt{G(0)}\;\tilde{f}_1 \exp(-i\tilde{\xi}_1) + \sqrt{G(\alpha)}\; f_2 \exp(-i\tilde{\xi}_2)\right| ,$$

$$\tilde{v} = \frac{180\lambda}{B\sqrt{4\pi}} \; C\left|\sqrt{g(0)}\;\tilde{f}_1 \exp(-i\tilde{\xi}_1) + \sqrt{g(\alpha)}\; f_2 \exp(-i\tilde{\xi}_2)\right| .$$

$\tilde{v}$ is thus a function of random variables $\tilde{\alpha}$, $\tilde{\eta}$, $\tilde{\xi}_1$, and $\tilde{\xi}_2$, or

$$\tilde{v} = \frac{180\lambda}{B\sqrt{4\pi}} \; C\left|\Omega(\tilde{\alpha},\tilde{\eta},\tilde{\xi}_1,\tilde{\xi}_2)\right| \quad .$$

$$\Omega = \sqrt{g(0)}\;\tilde{f}_1 \exp(-i\tilde{\xi}_1) + \sqrt{g(\alpha)}\; f_2 \exp(-i\tilde{\xi}_2) \quad .$$

The expected value of $\tilde{v}$ is found by taking the ensemble average over random variable spaces α, η, ξ_1, and ξ_2:

$$\tilde{v} = \frac{180\lambda}{B\sqrt{4\pi}} \; C\langle|\Omega(\tilde{\alpha},\tilde{\eta},\tilde{\xi}_1,\tilde{\xi}_2|\rangle \quad .$$

The form of this expression for $\langle\tilde{v}\rangle$ is not integrable in general. However, two useful properties of the kernel, $|\Omega|$, will enable an approximation to be invoked which results in an integrable form. First, the magnitude of the kernel $|\Omega|$ is large compared to the size of the expected fluctuations of Ω. This condition is due to the fact that the development of the model was based upon the weak scattering assumption. Second, the kernel $|\Omega|$ is slowly varying over the domains of α, η, ξ_1, and ξ_2. For example, with η, ξ_1, and ξ_2 fixed, let $\tilde{\alpha}$ vary over its range. The fluctuation which $\tilde{\alpha}$ imposes on Ω as it varies, and hence the fluctuation of $|\Omega|$, will be proportional to $|\sqrt{g(\alpha)}|$, a smooth function across the fluctuation domain. Similar observations may be made as $|\Omega|$ varies in η as $|\tilde{f}_1|$, in ξ_1 as $|\exp(-i\tilde{\xi}_1)|$, and in ξ_2 as $|\exp(-i\tilde{\xi}_2)|$.

It may be shown (Reference [36]) that the first moment of a function of a random variable may be approximated by the function of the first moment of that random variable under the two conditions mentioned above. In this case Ω is a random variable which is a function itself of independent random variables η, α, ξ_1, and ξ_2 and has a well defined moments. Assuming that the small fluctuation and smoothness conditions are met and noting that the function of Ω is absolute value, then

$$\langle|\Omega|\rangle = \langle[\Omega\Omega^*]^{1/2}\rangle \quad .$$

Assuming this to be the case in the expression for $\langle\tilde{v}\rangle$:

$$\langle\tilde{v}\rangle = \frac{180\lambda}{B\sqrt{4\pi}} \; C\langle|\Omega(\tilde{\alpha},\tilde{\eta},\tilde{\xi}_1,\tilde{\xi}_2)|\rangle$$

$$\langle\tilde{v}\rangle = \frac{180\lambda}{B\sqrt{4\pi}} \; C\langle|\sqrt{g(0)}\,\tilde{f}_1\exp(-i\tilde{\xi}_1) + \sqrt{g(\alpha)}\,f_2\exp(-i\tilde{\xi}_2)|\rangle,$$

$$\langle\tilde{v}\rangle = \frac{180\lambda}{B\sqrt{4\pi}} \; C\langle[(\sqrt{g(0)}\tilde{f}_1)^2 + (\sqrt{g(\alpha)}f_2)^2 + \tilde{f}_1 f_2\exp(-i\tilde{\xi}_1+i\tilde{\xi}_2)g(\alpha)$$

$$+g(\alpha)\tilde{f}_1 f_2\exp(+i\tilde{\xi}_1-i\tilde{\xi}_2)]^{1/2}\rangle,$$

the ensemble average may be taken as very nearly equal to the averages of the constituents of the absolute value process -

$$\langle\tilde{v}\rangle = \frac{180\lambda}{B\sqrt{4\pi}} \; C[\langle\sqrt{g(0)}\tilde{f}_1\rangle^2 + \langle\sqrt{g(\alpha)}f_2\rangle^2 + \langle\tilde{f}_1 f_2\exp(-i\tilde{\xi}_1+i\tilde{\xi}_2)g(\alpha)\rangle$$

$$\langle g(\alpha)\tilde{f}_1 f_2\exp(+i\tilde{\xi}_1-i\tilde{\xi}_2)\rangle]^{1/2} \quad .$$

The ensemble averages include integration on ξ_1 and ξ_2 taken over the domains $-\pi/2$ to $\pi/2$. Since $\tilde{\xi}_1$ and $\tilde{\xi}_2$ are uniformly distributed over this range, the last two ensembles are zero. Integration on the remaining two terms involves α over the domain 0 to π, and integration on η from $-\infty$ to ∞. Explicitly,

$$\langle \tilde{v} \rangle = \frac{180\lambda}{B\sqrt{4\pi}} \; C\left[\left(\int_{-\infty}^{\infty}\int_{0}^{\pi} \sqrt{g(0)}\,\eta\, h_\eta(r_i)\delta(\alpha)\,d\alpha d\eta\right)^2 + \left(\int_{-\infty}^{\infty}\int_{0}^{\pi} \sqrt{g(\alpha)}\, f_2 \delta(\eta) h_\alpha(\alpha)\,d\alpha d\eta\right)^2\right]^{1/2} .$$

The integration of the delta functions gives:

$$\langle \tilde{v} \rangle = \frac{180\lambda}{B\sqrt{4\pi}} \; C\left[\left(\int_{-\infty}^{\infty} \sqrt{g(o)}\,\eta\, h_\eta(\eta)\,d\eta\right)^2 + \left(\int_{0}^{\pi} \sqrt{g(\alpha)}\, f_2 h_\alpha(\alpha)\,d\alpha\right)^2\right]^{1/2} .$$

Using the fact that $g(\alpha=0)=1$ and f_2 is independent of α and has mean $\bar{f}_2$, substitute the expressions for $g(\alpha)$, h_η, and h_α:

$$\langle \tilde{v} \rangle = \frac{180\lambda}{B\sqrt{4\pi}} \; C\left[\left(\frac{1}{\sqrt{2\pi}\sigma_1}\int_{-\infty}^{\infty} \eta\, \exp[-(\eta-\bar{f}_1)^2/2\sigma_1^2]\,d\eta\right)^2 + \left(\bar{f}_2\int_{0}^{\pi} \exp\left[-\frac{\alpha^2 4\ell n2}{2B^2}\right]\frac{\alpha}{\sigma_2^2}\exp\left[-\frac{\alpha^2}{2\sigma_2^2}\right]d\alpha\right)^2\right]^{1/2} .$$

Random variable $\tilde{f}_1$ has been replaced by its dummy amplitude random variable, that is η. The first integral is the mean of a Gaussian random variable $\tilde{f}_1$, i.e. $\bar{f}_1$, and the second integral may be rewritten so that:

$$\langle \tilde{v} \rangle = \frac{180\lambda}{B\sqrt{4\pi}} \; C\left[\bar{f}_1^2 + \left(\bar{f}_2\int_{0}^{\pi} \frac{\alpha}{\sigma_2^2}\exp\left[-\frac{(4\ell n2\;\sigma_2^2+B^2)\alpha^2}{2\sigma_2^2 B^2}\right]d\alpha\right)^2\right]^{1/2} .$$

We have assumed that $\alpha << 1$ radian, so there will be negligible contribution to the integral on α over the range $\pi < \alpha < \infty$. Therefore, let the upper limit of integration go to infinity and define:

$$\frac{1}{2A^2} = \frac{4\ell n 2\sigma_2^2 + B^2}{2\sigma_2^2 B^2} \quad .$$

For a Rayleigh distribution,

$$1 = \frac{1}{A^2} \int_0^\infty \alpha \exp[-\alpha^2/2A^2] d\alpha$$

$$A^2 = \int_0^\infty \alpha \exp[-\alpha^2/2A^2] d\alpha .$$

Rewrite the integral in the expression for <v> in terms of A:

$$\langle \tilde{v} \rangle = \frac{180\lambda}{B\sqrt{4\pi}} \; C\left[\bar{f}_1^2 + \left(\frac{\bar{f}_2}{\sigma_2^2} \int_0^\infty \alpha \exp[-\alpha^2/2A^2] d\alpha\right)^2\right]^{1/2} \quad .$$

One immediately notes that the integral may be replaced by A^2:

$$\langle \tilde{v} \rangle = \frac{180\lambda}{B\sqrt{4\pi}} \; C\left[\bar{f}_1^2 + \left(\bar{f}_2 \frac{A^2}{\sigma_2^2}\right)^2\right]^{1/2} \quad .$$

Substituting in the definition for A^2, the first moment of v is:

$$\langle \tilde{v} \rangle = \frac{180\lambda}{B\sqrt{4\pi}} \; C\left[\bar{f}_1^2 + \bar{f}_2^2 \left(\frac{B^2}{4\ell n 2\sigma_2^2 + B^2}\right)^2\right]^{1/2} \quad .$$

APPENDIX C
SECOND MOMENT OF $\tilde{v}$

With the receiver output voltage equal to:

$$\tilde{v} = \frac{180\lambda}{B\sqrt{4\pi}} \; C\sqrt{g(\alpha)}\left|[\tilde{f}_1\exp(-i\tilde{\xi}_1)+f_2\exp(-i\tilde{\xi}_2)]\cdot [\tilde{f}_1\exp(+i\tilde{\xi}_1)+f_2\exp(+i\tilde{\xi}_2)]\right|^{1/2},$$

$\tilde{v}^2$ may be written as:

$$\tilde{v}^2 = \frac{180^2\lambda^2}{B^2 4\pi} \; C^2 g(\alpha)\left|\tilde{f}_1^2+f_2^2+\tilde{f}_1 f_2\exp(-i\tilde{\xi}_1+i\tilde{\xi}_2)+\tilde{f}_1 f_2\exp(+i\tilde{\xi}_1-i\tilde{\xi}_2)\right|.$$

The second moment of $\tilde{v}$, namely the ensemble average of $\tilde{v}^2$ taken over random variables η, α, and ξ is:

$$\langle v^2\rangle = \frac{180^2\lambda^2}{B^2 4\pi} \; C^2 \left\langle g(\alpha)[\tilde{f}_1^2+f_2^2+\tilde{f}_1 f_2\exp(-i\tilde{\xi}_1+i\tilde{\xi}_2)+\tilde{f}_1 f_2\exp(+i\tilde{\xi}_1-i\tilde{\xi}_2)]\right\rangle .$$

Since $\tilde{f}_1$, f_2, $\tilde{\xi}_1$, and $\tilde{\xi}_2$ are statistically independent, we may write:

$$\langle v^2\rangle = \frac{180^2\lambda^2}{B^2 4\pi} \; C^2[\langle g(0)\tilde{f}_1^2\rangle+\langle g(\alpha)f_2^2\rangle+\langle g(\alpha)\tilde{f}_1 f_2\exp(-i\tilde{\xi}_1+i\tilde{\xi}_2)\rangle + \langle g(\alpha)\tilde{f}_1 f_2\exp(+i\tilde{\xi}_1-i\tilde{\xi}_2)\rangle] .$$

The integration on ξ_1 and ξ_2 is taken over $-\pi/2$ to $\pi/2$ and, since $\tilde{\xi}_1$ and $\tilde{\xi}_2$ are uniformly distributed, the last two averages are zero, so that:

$$\langle v^2\rangle = \frac{180^2\lambda^2}{B^2 4\pi} \; C^2[\langle g(0)\tilde{f}_1^2\rangle+\langle g(\alpha)f_2^2\rangle].$$

Rewriting $\langle v^2 \rangle$ in terms of the integrals and pdf's:

$$\langle \tilde{v}^2 \rangle = \frac{180^2\lambda^2}{B^2 4\pi} \; C^2 \left[\int_{-\infty}^{\infty} \int_{0}^{\pi} g(0)\eta^2 h_\eta(\eta)\delta(\alpha)\,d\alpha\,d\eta + \int_{-\infty}^{\infty} \int_{0}^{\pi} g(\alpha) f_2^2 h_\alpha(\alpha)\delta(\eta)\,d\alpha\,d\eta \right].$$

Integration of the delta functions gives:

$$\langle \tilde{v}^2 \rangle = \frac{180^2\lambda^2}{B^2 4\pi} \; C^2 \left[\int_{-\infty}^{\infty} \eta^2 h_\eta(\eta)\,d\eta + \int_{0}^{\pi} g(\alpha) f_2^2 h_\alpha(\alpha)\,d\alpha \right] .$$

Substituting the expressions for $h_\eta(\eta)$, $g(\alpha)$, and $h_\alpha(\alpha)$,

$$\langle \tilde{v}^2 \rangle = \frac{180^2\lambda^2}{B^2 4\pi} \; C^2 \left[\int_{-\infty}^{\infty} \frac{\eta^2}{\sqrt{2\pi}\sigma_1} \exp[-(\eta-\overline{f}_1)^2/2\sigma_1^2]\,d\eta \right.$$

$$\left. + \overline{f}_2^2 \int_{0}^{\pi} \exp\left[-\frac{\alpha^2 4\ell n2}{B^2}\right] \frac{\alpha}{\sigma_2^2} \exp\left[-\frac{\alpha^2}{2\sigma_2^2}\right] d\alpha \right] .$$

The first integral is the second moment of Gaussian variable $\tilde{f}_1$, or $\langle \tilde{f}_1^2 \rangle = \overline{f}_1^2(1+\sigma_1^2)$, and the upper integration limit on α may be taken to ∞, so that:

$$\langle \tilde{v}^2 \rangle = \frac{180^2\lambda^2}{B^2 4\pi} \; C^2 \left[\overline{f}_1^2(1+\sigma_1^2) + \overline{f}_2^2 \int_{0}^{\infty} \frac{\alpha}{\sigma_2^2} \exp\left[-\frac{(8\ell n2\sigma_2^2+B^2)\alpha^2}{2\sigma_2^2 B^2}\right] d\alpha \right] .$$

Let $\dfrac{1}{2A^2} = \dfrac{8\ell n2\sigma_2^2+B^2}{2\sigma_2^2 B^2}$.

For a Rayleigh distribution,

$$1 = \frac{1}{A^2} \int_0^\infty \alpha \exp[-\alpha^2/2A^2]d\alpha$$

$$A^2 = \int_0^\infty \alpha \exp[-\alpha^2/2A^2]d\alpha \ .$$

Rewrite the integral in the expression for $\langle \tilde{v}^2 \rangle$ in terms of A:

$$\langle \tilde{v}^2 \rangle = \frac{180^2\lambda^2}{B^2 4\pi} \ C^2 \left[\bar{f}_1^2(1+\sigma_1^2) + \frac{\bar{f}_2^2}{\sigma_2^2} \int_0^\infty \alpha \exp[-\alpha^2/2A^2]d\alpha \right] \ .$$

The integral may then be replaced by A^2:

$$\langle \tilde{v}^2 \rangle = \frac{180^2\lambda^2}{B^2 4\pi} \ C^2 \left[\bar{f}_1^2(1+\sigma_1^2) + \bar{f}_2^2 \frac{A^2}{\sigma_2^2} \right] \ .$$

Finally, substituting in the definition of A^2, one obtains:

$$\langle \tilde{v}^2 \rangle = \frac{180^2\lambda^2}{B^2 4\pi} \ C^2 \left[\bar{f}_1^2(1+\sigma_1^2) + \bar{f}_2^2 \left(\frac{B^2}{8\ell n 2\sigma_2^2 + B^2} \right) \right] \ .$$

APPENDIX D
MODEL SUMMARY

I. Intensity Functions

$$\langle \tilde{f}_1^2 \rangle + \langle f_2^2 \rangle = 1$$

$$\langle \tilde{f}_1^2 \rangle = \bar{f}_1^2 (1+\sigma_1^2)$$

$$f_2^2 = \bar{f}_2^2 = 1 - \exp[-L/L_o]; \quad L_o \sim 180\text{km}$$

L = path length (km) .

II. Variance Parameters

Amplitude Variance

$$\sigma_1^2 = 2.6 \times 10^{-7} \, f^{7/12}(\text{GHz}) \, L^{11/6}(\text{km}) \, .$$

Angle of Arrival Variance

$$\sigma_2^2 = 5.67 \times 10^{-6} \, L^{1.56}(\text{km}) \, d^{-1/3}(\text{m})$$

L = path length
d = circular aperture diameter
f = frequency .

III. Gain Reduction

$$R = 10 \log_{10} \frac{\langle v \rangle^2}{\langle v \rangle^2} \Bigg|_{\sigma_2^2=0 \text{ (no angle fluctuation)}}$$

$\langle v \rangle$ = ensemble average of receiver voltage

$$R = 10 \log_{10} \frac{\overline{f}_1^2 + \overline{f}_2^2 \left(\frac{B^2}{4\ell n 2\sigma_2^2 + B^2} \right)^2}{\overline{f}_1^2 + \overline{f}_2^2}$$

B = half power beamwidth in degrees assuming a Gaussian antenna pattern function.

IV. Received Signal Variance

$$S^2 = 10 \log_{10} \frac{\langle v^2 \rangle - \langle v \rangle^2}{\langle v \rangle^2}$$

$$S^2 = 10 \log_{10} \frac{\overline{f}_1^2 \sigma_1^2 + \frac{\overline{f}_2^2 B^2}{8\ell n 2\sigma_2^2 + B^2} - \overline{f}_2^2 \left(\frac{B^2}{4\ell n 2\sigma_2^2 + B^2} \right)^2}{\overline{f}_1^2 + \overline{f}_2^2 \left(\frac{B^2}{4\ell n 2\sigma_2^2 + B^2} \right)^2}$$

APPENDIX E

FADE DISTRIBUTION VARIANCE

If

$$S^2 = 10 \log_{10} \frac{\sum_{i=1}^{N} (V_i - \langle v \rangle)^2}{N \langle v \rangle^2}$$

is the definition of received signal variance, and we are interested in the variance of the log amplitude, denoted σ_ℓ^2, a transformation must be made. Let ℓ_i be defined as log amplitude by

$$\ell_i = 20 \log_{10} \frac{v_i}{\langle v \rangle} \quad .$$

If the fluctuations about $\langle v \rangle$ are small compared to the magnitude of $\langle v \rangle$, let

$$\frac{v_i}{\langle v \rangle} = 1 + \frac{v_i - \langle v \rangle}{\langle v \rangle} = 1 + A_i \quad ; \qquad A_i \ll 1.$$

Then,

$$\ell_i = 20 \log_{10} (1 + A_i)$$

may be approximated by

$$\ell_i \approx (20 \log_{10} e) \cdot A_i \quad .$$

If a function f(v) is normally distributed, with mean $\langle v \rangle$ and variance σ_v^2, the function kf(v), where k is a constant, is also Gaussian, having mean $k\langle v \rangle$ and variance $k^2\sigma_v^2$. From the definition of the log-amplitude,

$$\frac{v_i - \langle v \rangle}{\langle v \rangle} = \frac{1}{20 \log_{10} e} \ell_i = k\ell_i .$$

However, the term on the left is a function of v_i for which we have previously defined variance in dB as S^{2*}. Hence, if σ_ℓ^2 is the variance of ℓ_i,

$$S^2 = 10 \log_{10} \left[\left(\frac{1}{20 \log_{10} e} \right)^2 \sigma_\ell^2 \right]$$

$$S^2 = 20 \log_{10} \left(\frac{\sigma_\ell}{20 \log_{10} e} \right) .$$

Solving for σ_ℓ, the standard deviation of the log-amplitude,

$$\sigma_\ell = 20 \log_{10} e \cdot 10^{S^2/20} .$$

*Note:

$$\mathrm{Var} \left\{ \frac{v_i - \langle v \rangle}{\langle v \rangle} \right\} = \frac{1}{\langle v \rangle^2} \mathrm{Var} \left\{ v_i - \langle v \rangle \right\}$$

$$\mathrm{Var} \left\{ \frac{v_i - \langle v \rangle}{\langle v \rangle} \right\} = \frac{1}{\langle v \rangle^2} \mathrm{Var} \left\{ v_i \right\} \quad \text{for a symmetric density function.}$$

$$10 \log_{10} \mathrm{Var} \left\{ \frac{v_i - \langle v \rangle}{\langle v \rangle} \right\} = S^2 .$$